

Recursive Attitude and Rate Estimator (RARE)

by

Robert Louis Stephens

A Thesis submitted to
The Faculty of the School of Engineering and Applied Sciences

of

The George Washington University
in partial fulfillment of the requirements for the degree of
Master of Science

December, 2000

Thesis directed by
Professor Robert H. Tolson
Professor of Engineering and Applied Sciences

Abstract

With the use of multiple receivers, the orientation and the rate of change of the orientation of a spacecraft can be determined by measuring both the differential phase and differential phase rate (Doppler) of the Global Positioning System carrier signals. Previous works, demonstrate that the attitude of spacecraft was accurately estimated using a four-element, non-linear predictive filter. In this paper, the non-linear predictive filter has been extended to a seven-element, non-linear predictive filter. This extended predictive filter estimates both attitude and attitude angular rate. This new filter is called RARE, 'Recursive Attitude and Rate Estimator'. The elements of the state vector consist of both attitude (described by quaternions) and angular rates. The results of RARE indicate that the calculation of attitude and angular rate is depended on the accuracy of the differential Doppler measurement. It is shown that values of standard deviation of differential Doppler approximately 1/100 the standard deviation of differential phase are sufficient in determining an estimated state to a desired accuracy (greater than 95% as compared to actual state). A more efficient and accurate method of determining attitude and angular rate using an extended Kalman filter is presented. Comparisons of results, among the different algorithms, indicate that it would be beneficial to analyze and perfect an extended Kalman filter for determining attitude and angular rate. The extended Kalman filter allowed for a greater error in the measured differential Doppler signal and little effect was contributed by the error in the measured differential phase signal. The results indicate that GPS measured observations are a feasible alternative to more expensive guidance control instruments.

Acknowledgments

The author greatly appreciates the support of the George Washington University JIAFS program faculty and staff. A special thanks to my advisers Dr. Robert H. Tolson and Dr. Paul A. Cooper for all their helpful advice and assistance. Also, I would like to thank my friends and family, especially my parents James and Chris Stephens, for their support throughout the past two years. Finalmente, gracias a Justin Strickland y un agradecimiento muy especial a mi amor Margarita Núñez Jáuregui.

Table of Contents

Abstract.....	i
Acknowledgments	ii
Table of Contents	iii
List of Figures.....	vi
List of Tables	viii
Nomenclature	ix
Chapter 1 Introduction.....	1
Chapter 2 Background	3
2.1 Derivation of differential phase and differential phase rate.....	3
2.2 Non-linear predictive filter	5
2.3 Extended Kalman filter	8
Chapter 3 Development of Simulated External Input.....	11
3.1 Line of sight and line of sight rate vectors.....	11
3.2 Simulated sight line cone	12
3.3 Coordinate transformation	15
3.4 Spacecraft and GPS satellites.....	17
3.4.1 Spacecraft parameters	17
3.4.2 GPS parameters.....	18

3.5 Simulation process	18
Chapter 4 Development of a Non-Linear Predictive Filter.....	21
4.1 Information processing	21
4.2 Development of the model error vector	24
4.3 Derivation and testing of the slope	25
Chapter 5 Nominal Case Study	32
5.1 Performance and accuracy	32
5.1.1 RARE.....	33
5.1.2 ALLEGRO.....	38
5.1.3 Extended Kalman filter.....	40
5.2 Convergence	43
5.2.1 RARE.....	43
5.2.2 ALLEGRO.....	45
5.2.3 Extended Kalman filter.....	45
5.3 Efficiency.....	46
Chapter 6 Concluding Remarks	49
References.....	51
Appendix A.....	A1
Appendix B	B1
B.1 Gravity gradient.....	B1
B.2 Inertially fixed.....	B5

B.2.1 Inertially fixed spacecraft oscillating 1° about all axesB5

B.2.2 Inertially fixed spacecraft oscillating 5° about all axesB8

List of Figures

<u>Figure</u>	<u>Page</u>
Figure 2.1 Representation of phase difference between two antennas	3
Figure 3.1 Graphical representation of the line of sight vector	11
Figure 3.2 Representation of the line of sight cone	13
Figure 3.3 Total number of GPS satellite in sight	15
Figure 3.4 Representation of the coordinate transformation of spacecraft	16
Figure 3.5 Flow chart representation of the simulated process	19
Figure 4.1 Graphical representation of the prediction scheme	23
Figure 4.2 Comparison of accuracy of the series expansion	27
Figure 4.3 Effects of series truncation on accuracy	28
Figure 4.4 Simulated applied angular acceleration about all three axes.....	30
Figure 4.5 Simulated applied angular acceleration between 0 and 100 seconds	31
Figure 5.1 Evaluation of RARE without data noise and $\Delta t = 100$	34
Figure 5.2 Performance of RARE with data noise and $\beta = 1/50$	36
Figure 5.3 Performance of RARE with data noise and $\beta = 1/100$	37
Figure 5.4 Performance of ALLEGRO with $\Delta t = 100$ and no data noise.....	39
Figure 5.5 Performance of ALLEGRO with no data noise	40
Figure 5.6 Performance of the EKF with data noise and $\beta = 1/50$	41
Figure 5.7 Performance of the EKF with data noise and $\beta = 1/100$	42
Figure 5.8 Convergence of RARE with data noise and $\beta = 1/25$	44
Figure 5.9 Convergence of the EKF with data noise and $\beta = 1/25$	46

Figure 5.10 Data noise requirements in RARE to assure a $50 \mu rad / s$ rate recovery	47
Figure 5.11 Data noise requirements in the EKF to assure a $50 \mu rad / s$ rate recovery ...	48
Figure B.1 Performance of RARE with $\beta = 1/100$ and 1° oscillation	B2
Figure B.2 Performance of ALLEGRO with 1° oscillation	B3
Figure B.3 Performance of the EKF with $\beta = 1/100$ and 1° oscillation	B4
Figure B.4 Performance of RARE with $\beta = 1/100$ and 1° oscillation	B6
Figure B.5 Performance of ALLEGRO with 1° oscillation	B7
Figure B.6 Performance of RARE with $\beta = 1/100$ and 1° oscillation	B8
Figure B.7 Performance of RARE with $\beta = 1/100$ and 5° oscillation	B9
Figure B.8 Performance of ALLEGRO with 5° oscillation.....	B10

List of Tables

<u>Table</u>	<u>Page</u>
Table 3.1 Definition of orbit elements	17
Table 3.2 Orbital elements of the spacecraft	17
Table 3.3 Orbital elements of all the GPS satellites	18
Table 4.1 Comparison of the analytical solution verse finite difference solution	30
Table B.1 Performance of RARE with $\beta = 1/50$ and 1° oscillation	B2
Table B.2 Performance of the EKF with $\beta = 1/50$ and 1° oscillation	B4
Table B.3 Performance of the RARE with $\beta = 1/50$ and 1° oscillation	B5
Table B.4 Performance of the EKF with $\beta = 1/50$ and 1° oscillation	B7
Table B.5 Performance of RARE with $\beta = 1/50$ and 5° oscillation	B8
Table B.6 Performance of the EKF with $\beta = 1/50$ and 5° oscillation.....	B10

Nomenclature

<u>Symbol</u>	<u>Description</u>	<u>Units</u>
a	Semi-major axis	km
\bar{a}	Angular acceleration	$\frac{rad}{sec^2}$
\bar{a}_k	Angular acceleration in discrete form	$\frac{rad}{sec^2}$
a_{ss}	Angular acceleration skew symmetric matrix	$\frac{rad}{sec^2}$
$A(\hat{q})$	Attitude matrix	
\dot{A}	Attitude rate matrix	$\frac{rad}{sec}$
\bar{b}_l	Antenna baseline vector (l^{th} - subscript represents a specific baseline, $l = 1, 2, 3$)	λ
c_i	Component of calculated output vector	
\bar{d}	Determined model error vector	
\bar{d}_k	Determined model error vector in discrete form	
e	Eccentricity	
\bar{e}_x	x-unit vector for spacecraft (roll axis)	
\bar{e}_y	y-unit vector for spacecraft (pitch axis)	
\bar{e}_z	z-unit vector for spacecraft (nadir/yaw axis)	
f	Model vector	

G	Model error distribution matrix	
g	Column vectors of model error distribution matrix G	
H_{ij}	Jacobian matrix of partial derivatives for the EKF	
i	Inclination of the orbit	
J	GPS loss function	
k_k	Kalman gain matrix for the EKF	
L_g^k	k^{th} -order Lie derivative with respect to the g function	
P_i	Lowest order derivative of c_i in the non-linear filter	
P_1^-	Covariance matrix of the initial state vector for the EKF	
P_k^+	Updated covariance for the EKF	
\hat{q}	Quaternion	
\hat{q}_k	Quaternion in discrete form	
Q_k	State noise covariance matrix error for the EKF	
r_E	Radius of the earth	<i>km</i>
\bar{r}_{GPS}	Position vector of a GPS satellite	<i>km</i>
\bar{r}_n	Position vector of the n^{th} GPS satellite	<i>km</i>
$\ \bar{r}_n\ $	Magnitude of the position vector of the n^{th} GPS satellite	<i>km</i>
$\bar{r}_{S/C}$	Position vector of the spacecraft	<i>km</i>
$\ \bar{r}_{S/C}\ $	Magnitude of the position vector of the spacecraft	<i>km</i>

\bar{R}_{nSC}	Line of sight vector from the spacecraft to GPS #n	<i>km</i>
$\ \bar{R}_{nSC}\ $	Magnitude of LOS vector	<i>km</i>
\bar{V}_{nSC}	Line of sight rate vector from the spacecraft to GPS #n	$\frac{km}{sec}$
$\ \bar{V}_{nSC}\ $	Magnitude of LOS rate vector	$\frac{km}{sec}$
R_k	Measured covariance matrix for the EKF	
\hat{s}	Line of sight unit vector	
\hat{s}_k	Line of sight unit vector in discrete form	
$\dot{\hat{s}}$	Line of sight rate vector	$\frac{1}{sec}$
$\dot{\hat{s}}_k$	Line of sight rate vector in discrete form	$\frac{1}{sec}$
$S[\hat{x}]$	Sensitivity matrix in non-linear filter	
t	Time	<i>sec</i>
t_k	Time at the beginning and end of interval k	<i>sec</i>
Δt	Interval of time, (time step)	<i>sec</i>
W	Weighting matrix	
\hat{x}	State vector	
\hat{x}_k	State vector in discrete form	
\bar{y}	Measured observational vector	
\bar{y}_k	Measured observational vector in discrete form	
\hat{y} or $\hat{c}(\hat{x}(t))$	Calculated output vector	

\hat{Y}_k^- Calculated output vector in discrete form before measurement

\hat{Y}_k^+ Calculated output vector in discrete form after measurement

$\hat{z}[\hat{x}, \Delta t]$ Correction term in non-linear filter

\hat{z}_k Observation vector for the EKF

<u>Greek Symbol</u>	<u>Description</u>	<u>Units</u>
β	Standard deviation ratio σ_P / σ_D	
λ	Signal wavelength	<i>cm</i>
λ_{ii}	Elements of diagonal Δt matrix in the non-linear filter	<i>sec</i>
$\Lambda(\Delta t)$	Diagonal Δt matrix in the non-linear filter	<i>sec</i>
$\Delta\phi$	Measured fractional phase difference or differential phase	λ
$\Delta\dot{\phi}$	Measured phase rate difference or differential Doppler	$\frac{\lambda}{\text{sec}}$
Φ_k	Recursive relationship in the EKF	<i>rad</i>
σ_D	Standard deviation in differential Doppler	$\frac{\lambda}{\text{sec}}$
σ_P	Standard deviation in differential phase	λ
θ	Angle between a baseline and the line of sight	<i>rad</i>
θ_{MAX}	Maximum angle between a position vector of a GPS satellite and the position vector of the spacecraft	<i>rad</i>

$\theta(t)$	Argument of latitude at epoch	<i>rad</i>
Ω	Right ascension of the ascending node	<i>rad</i>
$\Omega(\bar{a}_k)$	4 x 4 skew symmetric matrix for \bar{a}_k	$\frac{rad}{sec^2}$
$\Omega(\bar{\omega}_k)$	4 x 4 skew symmetric matrix for $\bar{\omega}_k$	$\frac{rad}{sec}$
ν	True anomaly	<i>rad</i>
$\hat{\nu}$	Measured error in signal vector (contains both differential phase and differential Doppler).	
ν_P	Measured error in differential phase signal	λ
ν_D	Measured error in differential Doppler signal	$\frac{\lambda \cdot rad}{s}$
ω	Argument of periapsis	<i>rad</i>
$\bar{\omega}$	Angular rate	$\frac{rad}{sec}$
$\bar{\omega}_k$	Angular rate in discrete form	$\frac{rad}{sec}$
ω_{ss}	Angular rate skew symmetric matrix measured in the spacecraft's body	$\frac{rad}{s}$

Acronym

Description

RARE	Recursive Attitude and Rate Estimator
ALLEGRO	Attitude Lean Loping Estimator using GPS Recursive Operations
EKF	Extended Kalman Filter
GPS	Global Positioning System

LOS	Line of Sight
DCM	Direction Cosine Matrix
STD	Standard Deviation
S/C	Spacecraft
L1	GPS carrier signal frequency (1575.42 MHz)

Chapter 1 Introduction

Phase difference measurements from Global Positioning System (GPS) signals provide a novel method for the determination of the attitude of a vehicle. The most widely used techniques for attitude determination involves methods that involve finding a proper orthogonal matrix that minimizes the scalar weighted norm-squared residual between sets of 3×1 body vector observations and 3×1 inertial vector observations mapped into the body frame. Many methods have been developed that solve this problem accurately and efficiently. However, the GPS observation is not in the form of a vector observation, so finding the attitude using GPS signals is inherently more difficult. The most recently introduced technique for attitude determination is based on a predictive filter scheme for nonlinear systems (ref. 1). This scheme uses a recursive (one time-step ahead) method to “predict” the required model error so that the propagated model produces optimal estimates. The specific name of the algorithm using GPS signals is ALLEGRO (Attitude-Lean-Loping-Estimator using GPS Recursive Operations). This paper will discuss the application of an extended non-linear predictive filter in the determination/estimation of the attitude and angular rate of a spacecraft using measurements of the GPS carrier signal. The use of this non-linear predictive filter will show that GPS measured observations are a feasible alternative to more expensive guidance control instruments aboard low Earth orbiting spacecrafts. The rate gyro is one possible instrument that may be replaced by this filtering method. In the previous algorithm, ALLEGRO, a four element state vector was sufficient in determining the attitude of a spacecraft rotating at a constant rate. The determination of attitude was accomplished by using the differential phase measurements of the GPS carrier wave at

several receivers. However, in this paper the procedure is modified to estimate a seven-element state vector consisting of a quaternion and an angular rate vector. This process requires that differential phase and differential phase rate (differential Doppler) measurements be taken. The name of the algorithm developed herein is RARE (Recursive Attitude and Rate Estimator). The direct measure of differential Doppler allows a more accurate method for measuring attitude of a spacecraft with non-zero angular accelerations. The filter is derived using two different approaches; the first approach is outlined in Chapter 2 and is based on the derivation and approximations used by Crassidis (ref. 1). In the second approach the filter is derived with the use of mathematical fundamentals. These mathematical fundamentals will be touched upon in Chapter 4. A procedure based on an extended Kalman filter is also developed. All methods are compared and contrasted for convergence time, robustness, and accuracy. Comparisons are made for several parameter variations including noise, initial state vector guess and acceleration.

Chapter 2 Background

This chapter briefly discusses the background of the GPS phase difference and Doppler difference measurements. Also discussed in this chapter are past methods for attitude determination.

2.1 Derivation of differential phase and differential phase rate

In this section, a brief description of the phase difference and phase rate difference measurements are shown. The phase difference is the measured difference in wavelengths between two GPS antennas, one master and one slave. Figure 2.1 below depicts the phase difference of the GPS signal (in red) received from two antennas separated by a baseline vector.

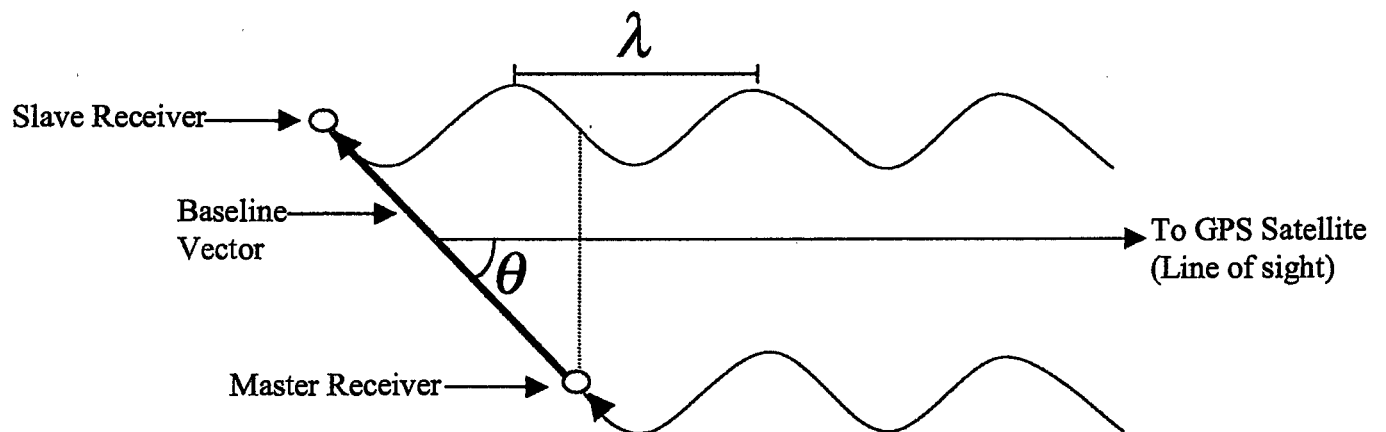


Figure 2.1 Representation of phase difference between two antennas

The phase difference is obtained by

$$b_i \cos(\theta) = \lambda(\Delta\phi - n) \quad (2-1)$$

where b_i represents the magnitude of the baseline vector, θ is the angle between the baseline vector and the line of sight vector as shown above, λ is the wavelength of the GPS signal, $\Delta\phi$ is the fractional phase difference between the two receivers, $0 \leq \Delta\phi \leq 1$

and n is the integer part of the phase difference. The GPS frequency carrier used is L1 at 1575.42 MHz. With the assumption that the integer offset is known, the measured fractional phase difference ($\Delta\phi$) can be expressed by

$$\Delta\phi = \bar{b}^T A \hat{s} + \nu_p \quad (2-2)$$

where \hat{s} is the unit line of sight vector in the inertial frame, A is a direction cosine matrix (the attitude matrix), \bar{b} is the baseline vector in the body-fixed frame and ν_p is the measurement error in the phase signal. The differential phase rate (differential Doppler) is the time derivative of the differential phase and is expressed by

$$\Delta\dot{\phi} = \bar{b}^T \dot{A} \hat{s} + \bar{b}^T A \dot{\hat{s}} + \nu_D \quad (2-3)$$

Where \dot{A} and $\dot{\hat{s}}$ are the time derivatives of the direction cosine matrix and line of sight vector respectively and ν_D is the measurement error in the Doppler signal. Equation (2-3) is the direct calculation of differential Doppler, which is the difference between the Doppler shift at the master receiver and the selected slave receiver. For example, each GPS satellite continually broadcasts signals giving its location, at a carrier frequency (1575.42 MHz) that is set and controlled by precise atomic clocks. When a receiver on the spacecraft senses the signal, the measured frequency has been shifted because of the relative motion of the satellite and the GPS sending the signal. The rotational velocity of the spacecraft can be determined from the Doppler shift of the signal. Differencing the Doppler shift sensed by the master and a slave receiver results in the differential phase rate, which is better known as the differential Doppler. The variable \dot{A} in equation (2-3) can be represented by $[\omega \times]^T A$, where $[\omega \times]^T$ is a 3x3 skew symmetric matrix with the

angular rate measured in the spacecraft's body fixed coordinate system (Appendix A).

The observation vector output is

$$\tilde{y} = \begin{bmatrix} \Delta\phi \\ \Delta\dot{\phi} \end{bmatrix} = \begin{bmatrix} \bar{b}^T A \hat{s} + v_p \\ \bar{b}^T \dot{A} \hat{s} + \bar{b}^T A \dot{\hat{s}} + v_D \end{bmatrix}. \quad (2-4)$$

2.2 Non-linear predictive filter

In this section, a non-linear predictive filter will be discussed and a general expression for the model error vector will be derived (see refs. 1 and 2 for more details). In a non-linear predictive filter it is assumed that the state, \hat{x} and output, \hat{y} , estimates are given by a preliminary model and a to-be-determined model error vector, given by

$$\begin{aligned} \dot{\hat{x}}(t) &= f(\hat{x}(t)) + G(\hat{x}(t)) \bar{d}(t) \\ \hat{y}(t) &= \hat{c}(\hat{x}(t)) \end{aligned} \quad (2-5)$$

where f is the model vector, G is the model-error distribution matrix, \bar{d} is the to be determined model error vector, and \hat{c} is the calculated output estimate vector. Equation (2-4) can be rewritten in terms of equation (2-5) and is given by

$$\tilde{y}(t) = \hat{c}(\hat{x}(t)) + \hat{v} \quad (2-6)$$

where \hat{v} is a 2 x 1 vector containing the measurement error on differential phase and differential Doppler. To determine f and G in equation (2-5), write equation (2-5) in discrete form and expand \hat{x}_{k+1} in a second order Taylor series expansion, solve for $\dot{\hat{x}}_k$, and substitute the results into the discrete form of equation (2-5). The definition of the model error vector determines the order of the Taylor series. For ALLEGRO the model error vector is defined as angular rate and is assumed constant during a time step. For this reason a first order Taylor series expansion was sufficient. For RARE a second order

series expansion is used since the model error vector is defined as a constant angular acceleration rather than a constant angular rate during a time step. Once f and G are known, a recursive relation from $\hat{x}(t_k) \rightarrow \hat{x}(t_{k+1})$ can be written. The next step in the non-linear filter method is to derive a model error vector. In deriving a model error vector, a GPS loss function is used, given by

$$J = \frac{1}{2} \{ \tilde{y}(t_{k+1}) - \hat{y}(t_{k+1}) \}^T R^{-1} \{ \tilde{y}(t_{k+1}) - \hat{y}(t_{k+1}) \} + \frac{1}{2} \bar{d}^T(t_k) W \bar{d}(t_k) \quad (2-7)$$

where $\tilde{y}(t_{k+1})$ is defined in equation (2-4), $\hat{y}(t_{k+1})$ is defined in equation (2-8) below, R is the positive definite covariance matrix, W is a weighting matrix, and $\bar{d}(t_k)$ is the to be determined model error vector. Before the model error vector can be determined, $\hat{y}(t_{k+1})$ has to be expanded in a Taylor series. The expansion is given by

$$\hat{y}(t + \Delta t) \approx \hat{y}(t) + \hat{z}[\hat{x}(t), \Delta t] + \Lambda(\Delta t) S[\hat{x}(t)] \bar{d}(t) \quad (2-8)$$

where the i^{th} element of $\hat{z}[\hat{x}(t), \Delta t]$ is given by

$$\hat{z}_i[\hat{x}(t), \Delta t] = \sum_{k=1}^{p_i} \frac{\Delta t^k}{k!} L_f^k(c_i) \quad (2-9)$$

where p_i , $i=1,2,\dots,m$, is the lowest order of the derivative of $c_i[\hat{x}(t)]$ in which any component of $\bar{d}(t)$ first appears due to successive differentiation and substitution for $\dot{\hat{x}}(t)$ on the right hand side. For the RARE algorithm, $p_1=2$ and $p_2=1$ since c_1 requires two successive differentiations and c_2 only requires one. $L_f^k(c_i)$ is an k^{th} -ordered Lie derivative, defined by

$$L_f^k(c_i) = c_i \quad \text{for} \quad k = 0$$

$$L_f^k(c_i) = \frac{\partial L_f^{k-1}(c_i)}{\partial \hat{x}} f \quad \text{for } k \geq 1$$

where f is an $n \times 1$ array given in equation (2-5). $\Lambda(\Delta t)$ is a diagonal matrix with elements given by

$$\lambda_{ii} = \left[\frac{\Delta t^{p_i}}{p_i!} \right], \quad i = 1, 2, \dots, m$$

$S[\hat{x}(t)]$ is a generalized sensitivity matrix for non-linear systems with each i^{th} row given by

$$S_i = \left\{ L_{g_1} [L_f^{p_i-1}(c_i)], \dots, L_{g_q} [L_f^{p_i-1}(c_i)] \right\}, \quad i = 1, 2, \dots, m$$

where the Lie derivative with respect to L_{g_j} is defined by

$$L_{g_j} [L_f^{p_i-1}(c_i)] \equiv \frac{\partial L_f^{p_i-1}(c_i)}{\partial \hat{x}} g_j, \quad j = 1, 2, \dots, q$$

where g_j is the j^{th} column of the matrix $G[\hat{x}(t)]$ given in equation (2-5). Once equation (2-8) is calculated and substituted into equation (2-7), the variation of the loss function is set equal to zero, and solved for the model error vector. Also a constant sampling rate is assumed so that $\tilde{y}(t_{k+1}) \equiv \tilde{y}_{k+1}$. The resulting model error solution is

$$\bar{d}_k = - \left[\Lambda(\Delta t) S(\hat{x}_k) \right]^T R^{-1} \Lambda(\Delta t) S(\hat{x}_k) + W \right]^{-1} \left[\Lambda(\Delta t) S(\hat{x}_k) \right]^T R^{-1} [\hat{z}(\hat{x}_k, \Delta t) - \tilde{y}_{k+1} + \hat{y}_k] \quad (2-10)$$

Therefore, given a state estimate at time t_k , equation (2-8) can be used to process the measurements at t_{k+1} . The weighting matrix W serves to weight the relative importance between the propagated model and measured quantities. If this matrix is set to zero, then no weight is placed on minimizing the model corrections so that a memoryless estimator

is given. This solution is rederived in Chapter 4 using a different relationship for the state, \hat{x} , in place of the truncated Taylor series approximation (see also ref.2).

2.3 Extended Kalman filter

The Kalman filter addresses the general problem of estimating the state of a first order, discrete time process that is governed by a linear difference equation. For the case of RARE, the process to be estimated and/or the measurement relationship to the process are non-linear. A Kalman filter that is linearized about the current mean and covariance is referred to as an extended Kalman filter or EKF. The EKF requires linearization of the estimation in the vicinity of the current estimate using the partial derivatives of the process and measurement functions to compute estimates even in the face of non-linear relationship (refs. 3 and 4). Three covariance matrices are required. The first is P_k^- which describes the covariance of the state vector \hat{x}_k^- at step k. The covariance matrix for RARE is a 7x7 matrix. The second and third covariance matrices describe the covariance of the errors and are define as Q_k and R_k . The matrix R_k is a 2x2 diagonal matrix of the covariance of the measurement. The matrix Q_k is a 7x7 diagonal state noise matrix. This matrix is used to tune the extended Kalman filter and the elements are chosen so that the result is optimized. In the EKF the propagation equation is given by

$$\hat{x}_{k+1} = \Phi_k \hat{x}_k + \hat{v}_k \quad (2-11)$$

where Φ_k is the recursive relationship between $\hat{x}(t_k)$ and $\hat{x}(t_{k+1})$ and $\hat{v}_k \in Q_k$ represents the process noise. The observational equation is given by

$$\hat{z}_k = \hat{c}(\hat{x}_k) + \mu_k \quad (2-12)$$

where \hat{c} is the estimated output vector and $\mu_k \in R_k$ represents the measurement noise.

Once all the initial inputs are chosen, the Jacobian matrix of partial derivatives can be assemble and is defined as

$$H_{ij} = \frac{\partial c_i}{\partial x_j} \quad (2-13)$$

where c_i is the calculated output estimate vector, defined in equation (2-8), and x_j is the initial state vector at t_k . Equation (2-13) is computed in the same manner as in the non-linear predictive filter only the assembly of the H_{ij} matrix differs. With all the above values calculated, the Kalman gain matrix is determined from the following relationship

$$K_k = P_k^- H_k^T (H_k P_k^- H_k^T + R_k)^{-1}. \quad (2-14)$$

The next step is to compute the updated state vector. The computation of the new state vector requires the sum of the initial state and the product of the Kalman gain matrix and the residual, given by

$$\hat{x}_k^+ = \hat{x}_k^- + K_k (\hat{z}_k - \hat{y}_k) \quad (2-15)$$

where \hat{y}_k is the calculated value defined in equation (2-5). The computation of the updated covariance matrix is given by

$$P_k^+ = (I - K_k H_k) P_k^- \quad (2-16)$$

where I is an identity matrix of the proper size. The computation of the projected state vector and covariance matrix P_{k+1}^- for the next time step completes the process of EKF.

The equations, which describe the projected conditions for the next time step, are given

by

$$P_{k+1}^- = \Phi_k P_k^+ \Phi_k^T + Q_k$$

and

(2-17)

$$\hat{x}_{k+1}^- = \Phi_k \hat{x}_k^+$$

where Φ_k is the recursive relationship between $\hat{x}(t_k)$ and $\hat{x}(t_{k+1})$ and Q_k is the covariance of the error and can be used to tune the covariance of the state and/or the filter. Using the new initial estimates in equation (2-17), the above process is repeated starting at equation (2-13).

Chapter 3 Development of Simulated External Input

In this chapter, the development of the LOS and LOS rate vectors between the spacecraft and each GPS satellite will be discussed. To determine these vectors at a given time, the orbital elements of the spacecraft and all the GPS satellites must be known. Once the orbital elements are known, a position and a velocity vector for the spacecraft and each GPS satellite can be found. The line of sight vector (\hat{s}) describes the magnitude and direction of a particular GPS satellite with respect to the spacecraft. The time rate of change of the LOS vector ($\dot{\hat{s}}$) is the rate at which the vector from the spacecraft to a GPS satellite changes. This is calculated by taking the time derivative of the LOS vector. Calculated data in this chapter are required as input for the RARE algorithm.

3.1 Line of sight and line of sight rate vectors

The line of sight is the vector, \hat{s} , from the center of mass of the spacecraft to the center of mass of each GPS satellite and is shown in Figure 3.1.

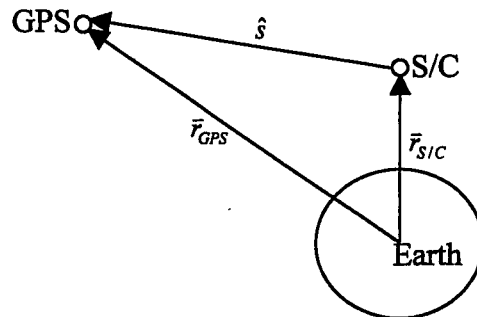


Figure 3.1 Graphical representation of the line of sight vector

The calculation of the line of sight vector is performed based on a geocentric inertial coordinate system.

The LOS unit vectors are given by

$$\hat{s} = \frac{\vec{r}_{GPS} - \vec{r}_{S/C}}{\|\vec{r}_{GPS} - \vec{r}_{S/C}\|} \quad (3-1)$$

Where $\vec{r}_{S/C}$ represents the position vector of the center of mass of the spacecraft, \vec{r}_{GPS} represents the position vector of the center of mass of a particular GPS. The line of sight rate vector is the time rate of change of \hat{s} and, in addition to the position vectors, requires the velocity vectors of the spacecraft and each GPS satellite. Applying the quotient rule to equation (3-1), the line of sight rate $\dot{\hat{s}}$ is given by

$$\dot{\hat{s}} = \frac{\vec{V}_{nsc}}{\|\vec{R}_{nsc}\|} - \frac{\vec{R}_{nsc}}{\|\vec{R}_{nsc}\|^3} (\vec{R}_{nsc} \cdot \vec{V}_{nsc}) \quad (3-2)$$

where \vec{R}_{nsc} is the difference between the position vectors of the spacecraft and a GPS satellite ($\vec{r}_{GPS} - \vec{r}_{S/C}$), \vec{V}_{nsc} is the relative velocity vector between the spacecraft and a GPS satellite $\vec{v}_{GPS} - \vec{v}_{S/C}$. The small n in the subscript of the above vectors represents the GPS satellite number.

3.2 Simulated sight line cone

The procedure followed in this section describes the simulated line of sight cone. The line of sight cone is defined as a region above the spacecraft where the receiver can measure the GPS signal. The antenna plane is defined as the plane where the receivers are mounted on the spacecraft. To avoid any interference from, for instance, the solar panels or any other S/C components, a LOS cone is formed on the antenna plane. Figure 3.2 illustrates the line of sight cone used in the simulations. In Figure 3.2, only GPS satellite #2 is in sight. GPS satellite #1 and #3 are out of sight of the spacecraft.

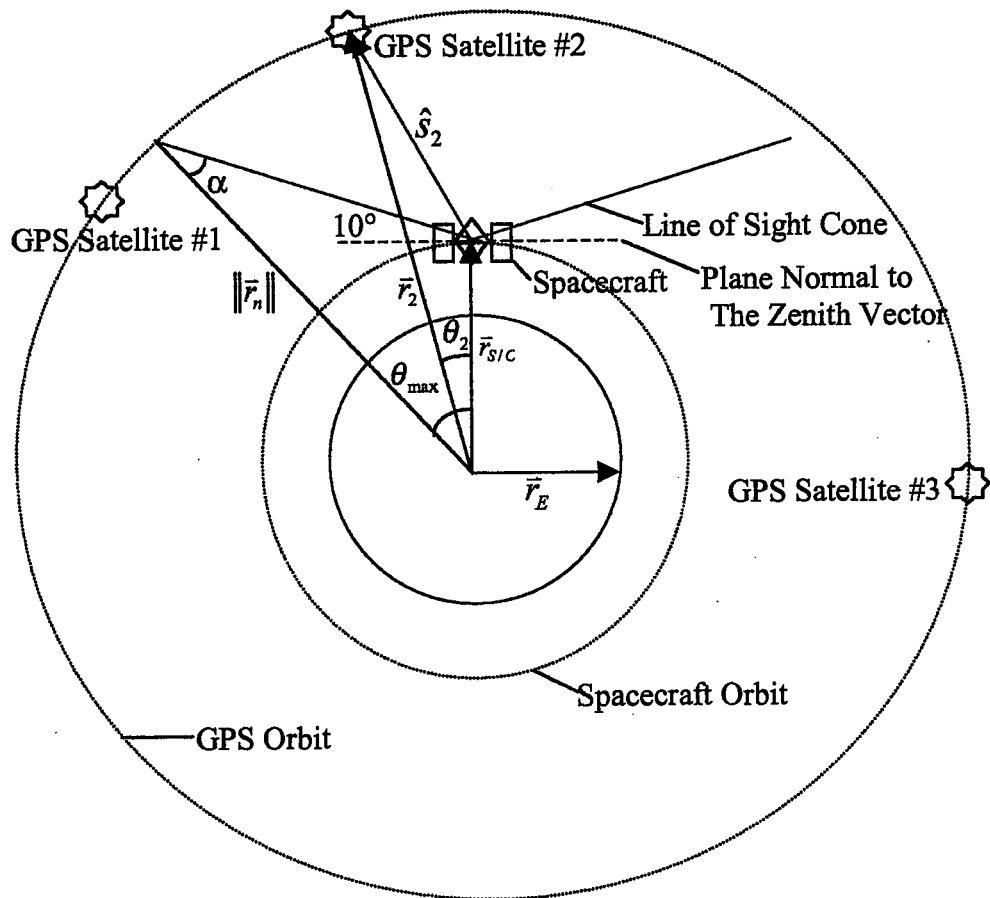


Figure 3.2 Representation of the line of sight cone

To determine if a GPS satellite is in sight of the spacecraft at a given time, the angle θ_n formed between the position vector of the spacecraft and the GPS satellite must be less than the angle θ_{MAX} . To determine the maximum angle, the law of sines is used for the plane triangle formed by the position vector of the spacecraft, the GPS satellite and the sight line cone. The magnitude of all the GPS satellite position vectors $\|\vec{r}_n\|$ can be assumed constant because they all have the same semi-major axis and are all nearly circular orbits. The angle formed between the position vector of the spacecraft and the

vector along the side of the sight line cone is 100° . With the two segments formed by the two position vectors and the before mentioned angle of 100° , the angle α can be found, and is given by

$$\alpha = \sin^{-1} \left(\frac{\|\vec{r}_{S/C}\|}{\|\vec{r}_n\|} \sin(100^\circ) \right) \cong 15^\circ.$$

Where the magnitude of the position vectors are

$$\begin{aligned} \|\vec{r}_{S/C}\| &= 6901km \\ \|\vec{r}_n\| &= 26609km \end{aligned}$$

Now that two angles of the plane triangle are known, the third angle, θ_{MAX} , is found using

$$\theta_{MAX} = 180 - (100^\circ + \alpha) \cong 65^\circ.$$

A simulation using the criterion explained above is tested over a period of 40 minutes. A plot of the number of available GPS satellites for the simulation is shown Figure 3.3. The particular situation described in Figure 3.3 will be assumed for all cases studied in this paper.

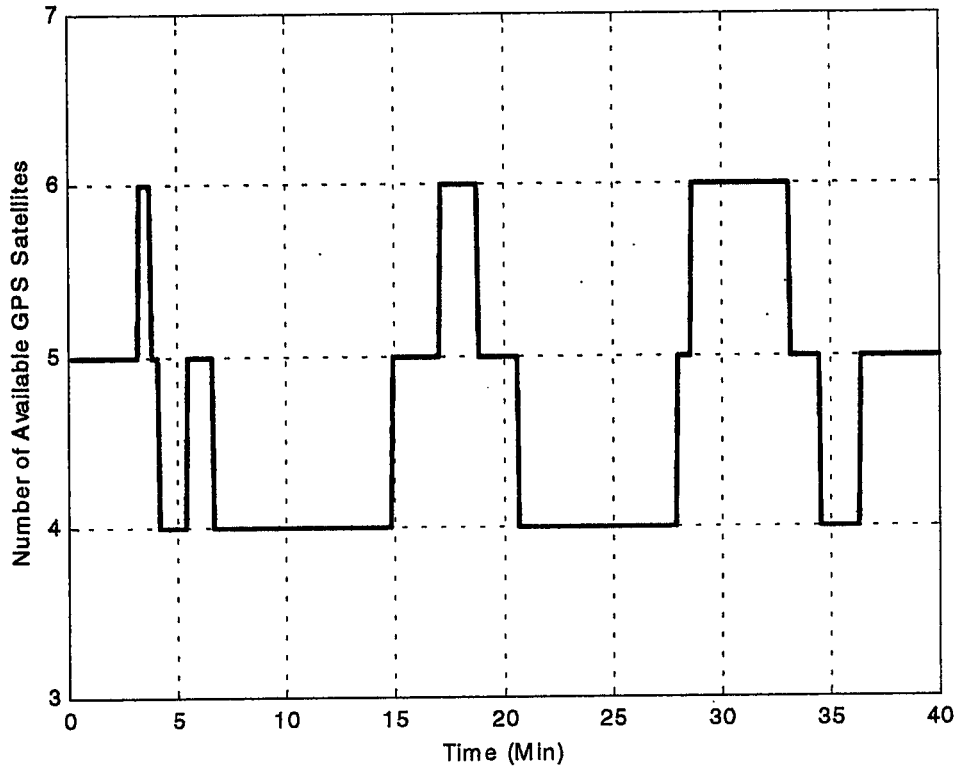


Figure 3.3 Total number of GPS satellite in sight

As shown in Figure 3.3, there are at least 4 GPS satellites within the LOS cone of the spacecraft all the time with a maximum of six available over the 40 minute interval.

3.3 Coordinate transformation

In this section, the computation of the direction cosine matrix relating the inertial frame to the spacecraft's body-fixed frame is discussed. The location of the spacecraft and all GPS satellites can be described using a 3-1-3 Euler angle set. These angles are shown in Figure 3.5 and are defined in orbital element terms. The first angle is the right ascension of the ascending node (Ω), the second is the inclination of the orbits (i), and the third is dependent on time and is the sum of the argument of periaapsis (ω) and true anomaly (ν). This third angle is known as the argument of latitude ($\theta(t)$). The 3-1-3 direction cosine

matrix will transform the coordinates from the inertial frame to the orbit frame. The orbital frame is shown in Figure 3.4 as \bar{e}_x , \bar{e}_y , and \bar{e}_z . Where the nadir is \bar{e}_z and is positive towards the center of earth, \bar{e}_y is positive along the negative normal of the orbital plane and \bar{e}_x is positive in the direction of the orbit determined from $\bar{e}_y \times \bar{e}_z$.

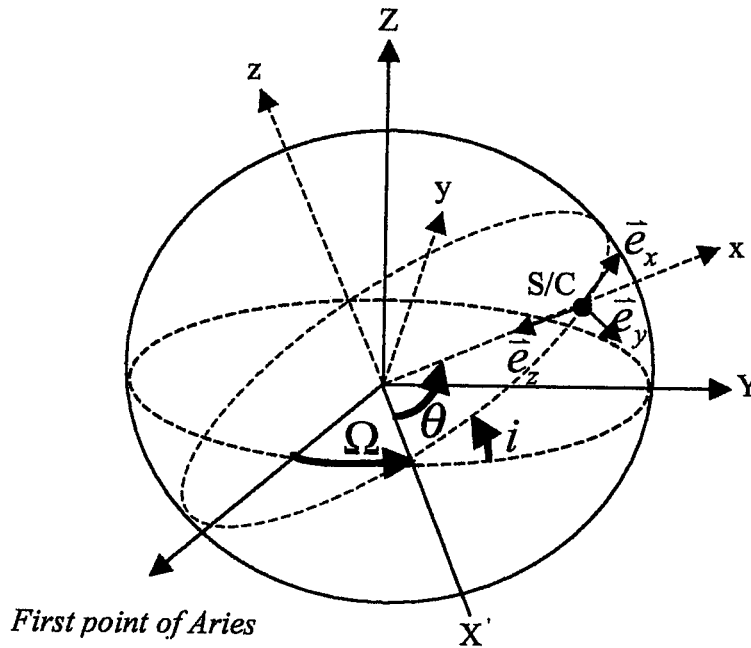


Figure 3.4 Representation of the coordinate transformation of spacecraft

The direction cosine matrix A is defined as

$$A = \begin{bmatrix} 0 & 1 & 0 \\ 0 & 0 & -1 \\ -1 & 0 & 0 \end{bmatrix} [\text{DCM}].$$

Where the first matrix is the rotation within the orbit reference frame and the second matrix is a standard 3-1-3 DCM. The A matrix is the attitude matrix and is in terms of quaternions (ref. 5).

3.4 Spacecraft and GPS satellites

The simulated motion profile was for an actual spacecraft, the Small Satellite Technology Initiative (SSTI) Lewis satellite, which was launched on August 22, 1997 (ref. 1). Although the spacecraft was lost, due to a malfunction shortly after the launch, the profile was used in all the algorithm simulations. The simulated motion profile for the GPS satellites used is from a previous 21-satellite constellation. Table 3.1 defines the symbols that represent each orbital element. More information on orbital elements can be found in (refs. 6 and 7).

Table 3.1 Definition of orbit elements

Symbols	Orbital element
a	Semi-major axis
e	Eccentricity
i	Inclination
Ω	Longitude of the ascending node
ω	Argument of periapse
ν	True anomaly at epoch

3.4.1 Spacecraft parameters

The orbital elements of the spacecraft are defined in Table 3.2.

Table 3.2 Orbital elements of the spacecraft

a	e	i	Ω	ω	ν
6901.137	0.0001	97.45	-157.1	0	208.8

The spacecraft has four GPS antennas that form three baselines. The baseline vector components, in wavelengths measured from the master antenna, are given by

$$\bar{b}_1 = \begin{bmatrix} 2.75 \\ 1.64 \\ -0.12 \end{bmatrix}, \bar{b}_2 = \begin{bmatrix} 0.00 \\ 6.28 \\ -0.17 \end{bmatrix}, \bar{b}_3 = \begin{bmatrix} -3.93 \\ 3.93 \\ -1.23 \end{bmatrix}$$

where the wavelength is approximately 0.19 meters.

3.4.2 GPS parameters

The Global Positioning System (GPS) satellite parameters used for the ALLEGRO, RARE, and EKF simulations are listed in Table 3.3. Note: Each GPS satellite is ordered from GPS #1 to GPS #21, as defined below.

Table 3.3 Orbital elements of all the GPS satellites

GPS #	a	e	i	Ω	ω	ν
1	26609	0	55	325.73	0	190.88
2	26609	0	55	325.73	0	329.88
3	26609	0	55	325.73	0	87.13
4	26609	0	55	25.73	0	260.88
5	26609	0	55	25.73	0	358.88
6	26609	0	55	25.73	0	129.88
7	26609	0	55	85.73	0	289.88
8	26609	0	55	85.73	0	68.88
9	26609	0	55	85.73	0	172.63
10	26609	0	55	145.73	0	328.13
11	26609	0	55	145.73	0	86.63
12	26609	0	55	145.73	0	216.88
13	26609	0	55	205.73	0	12.13
14	26609	0	55	205.73	0	108.88
15	26609	0	55	205.73	0	247.63
16	26609	0	55	265.73	0	42.88
17	26609	0	55	265.73	0	173.13
18	26609	0	55	265.73	0	291.63
19	26609	0	55	325.73	0	224.38
20	26609	0	55	205.73	0	150.88
21	26609	0	55	85.73	0	35.38

3.5 Simulation process

Section 2.1 derived equations (2-2) and (2-3) which describe the observed differential phase and phase rate. Sections 3.1 and 3.2 describe the methods used to calculate the LOS and LOS rate vectors. Section 3.3 shows the orbital elements that are used to determine the known attitude matrices. Also in section 3.3, the baseline vectors of the

spacecraft are presented. All of the values presented in sections 3.1 through 3.3 and the random noise are substituted into equations (2-2) and (2-3) to describe the simulated observed signal. Figure 3.5 represents the path that the entire process will follow.

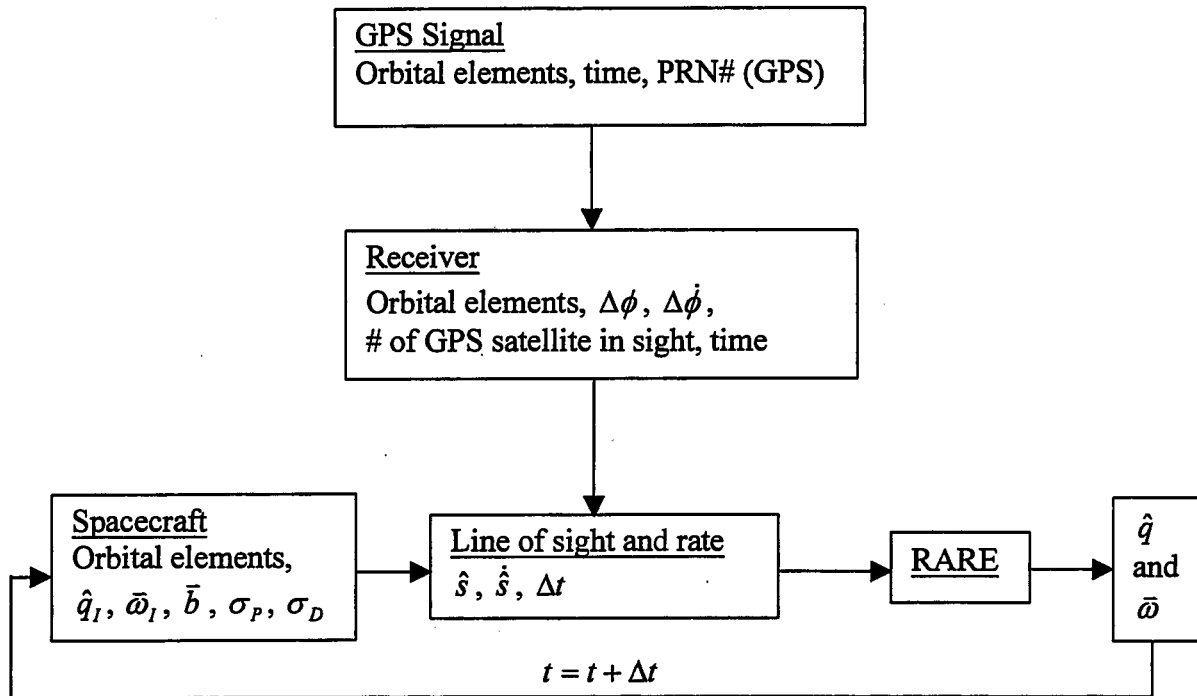


Figure 3.5 Flow chart representation of the simulated process

The flow chart in Figure 3.5 has two starting points. The first is the GPS satellite and the receiver, and the second is the spacecraft. The GPS receivers on board the spacecraft will extract all the ephemeris parameters from the GPS signal. These parameters include the time and all the orbital elements and GPS satellite numbers that the spacecraft receivers can detect. In addition to the ephemeris data, the receiver will also measure the differential phase and differential Doppler for each baseline and GPS satellite. The information from the spacecraft, GPS satellite, and receivers are sent into a function, which calculates the line of sight, line of sight rate, and the time interval being evaluated. The user inputs the information given by the spacecraft receivers. The user initially

estimates the attitude and angular rate. All this information is sent into RARE and an optimized state estimate is computed. This new state estimate becomes the initial guess for the quaternion and angular rate for the next interval of time.

Chapter 4 Development of a Non-Linear Predictive Filter

In this chapter, the algorithm RARE is derived using a predictive non-linear filter. The mathematics covering the matrix and vector derivatives is outlined in Appendix A. There are two approaches used to derive RARE. The first method is outlined by Crassidis (refs. 1 and 2) and was described in Chapter 2. The second method is based on using a different relationship for x_i in place of the truncated Taylor series approximation. The second approach is described in this chapter.

4.1 Information processing

The prediction scheme, shown in Figure 4.1, is a graphical representation and explanation of how the prediction is being made. The \hat{Y}_k^+ is the estimated output vector at some initial time t_k and is defined as

$$\hat{Y}_k^+ = \left[\begin{array}{c} \bar{b}^T A(\hat{q}_k) \hat{s}_k \\ \bar{b}^T [\bar{\omega}_k \times]^T A(\hat{q}_k) \hat{s}_k + \bar{b}^T A(\hat{q}_k) \hat{s}_k \end{array} \right], \quad (4-1)$$

where \hat{q}_k and $\bar{\omega}_k$ are the initial estimated value for the first iteration supplied by the user. The process starts by first calculating \hat{q}_{k+1} and $\bar{\omega}_{k+1}$, assuming that the acceleration for the first iteration is zero. The plus and minus signs in the superscript of some of the variables presented, indicate when the measurement is taken. The minus sign indicates the value before the measurement information is applied and the plus sign indicates the value after the measurement information is applied to update the estimate. Equation (4-2) represents the attitude rate and the angular acceleration given by

$$\begin{aligned} \dot{\hat{q}} &= \frac{1}{2} \Omega(\bar{\omega}) \hat{q} \\ \dot{\bar{\omega}} &= \bar{a} \end{aligned} \quad (4-2)$$

The attitude rate and angular acceleration are assumed to be adequately modeled by a constant model error vector \bar{a}_k between each measured time step (where \bar{a}_k represents the angular acceleration of the spacecraft). Equations (4-2) can be solved using two assumptions. First, the angular rate is assumed linear in time so that the angular acceleration is constant over each time step. Second, the change in the angle of rotation between the two different attitudes at t_k and t_{k+1} is assumed small (small angle approximation). The \hat{q}_{k+1} was determined using an integrating factor on the following equation

$$\dot{\hat{q}} - \frac{1}{2}\Omega(\bar{\omega})\hat{q} = 0. \quad (4-3)$$

Differencing and integrating equation (4-2) for the angular acceleration and solving equation (4-3), results in the two following prediction equations

$$\begin{aligned} \hat{q}_{k+1} &= e^{\left(\frac{\Delta t}{2}\Omega(\bar{\omega}_k) + \frac{\Delta t^2}{4}\Omega(\bar{a}_k)\right)} q_k \\ \bar{\omega}_{k+1} &= \bar{\omega}_k + \bar{a}_k \Delta t \end{aligned} \quad (4-4)$$

where

$$\Omega(\bar{\omega}_k) = \begin{bmatrix} 0 & -\omega_3 & \omega_2 & \omega_1 \\ \omega_3 & 0 & -\omega_1 & \omega_2 \\ -\omega_2 & \omega_1 & 0 & \omega_3 \\ -\omega_1 & -\omega_2 & -\omega_3 & 0 \end{bmatrix} \quad (4-5)$$

and

$$\Omega(\bar{a}_k) = \begin{bmatrix} 0 & -a_3 & a_2 & a_1 \\ a_3 & 0 & -a_1 & a_2 \\ -a_2 & a_1 & 0 & a_3 \\ -a_1 & -a_2 & -a_3 & 0 \end{bmatrix}.$$

Although this solution is not exact since Ω has multiple roots, the solution was compared with a finite difference solution of Equation (4-3) and gives acceptable accuracy within

the time span investigated. Equations (4-4) represent the update from t_k to t_{k+1} where $\bar{\omega}_k$ and \hat{q}_k are the initial values and are considered known. Once these new predicted values \hat{q}_{k+1} and $\bar{\omega}_{k+1}$ are found under the assumption that acceleration is zero for the first iteration, \hat{Y}_{k+1}^- can be determined using equation (4-1).

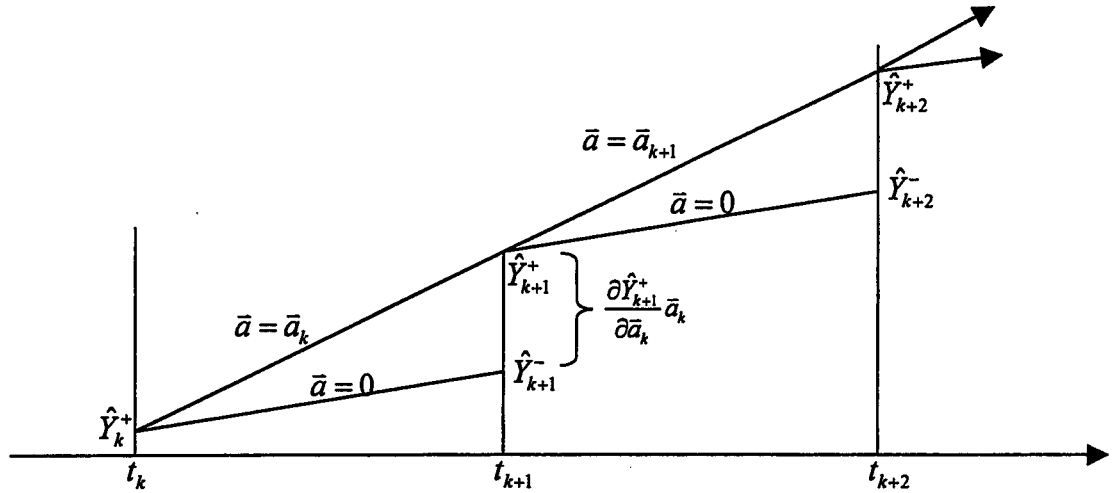


Figure 4.1 Graphical representation of the prediction scheme

The first iteration in RARE calculates \hat{Y}_{k+1}^- assuming that acceleration is zero. On the second iteration, acceleration is calculated. The calculated acceleration is called the model error vector. This acceleration is then used in equation (4-4) to up-date the state estimate vector \hat{Y}_{k+1}^+ . Additional iterations can be applied over the same time step, using the previous acceleration and will drive the system closer to the actual values of \hat{Y}_{k+1}^+ . This process is repeated for two or more iterations over each time interval from t_k to t_{k+1} and is repeated until defined to stop. The process is shown in Figure 4.1.

4.2 Development of the model error vector

An equation for the model error vector is obtained by minimizing the GPS loss function. The loss function consists of the weighted sum square of the measurement minus estimate residuals plus the weighted sum square of the model correction term, given by

$$J = \frac{1}{2} \left\{ \tilde{Y}(t_{k+1}) - \hat{Y}^+(t_{k+1}) \right\}^T R^{-1} \left\{ \tilde{Y}(t_{k+1}) - \hat{Y}^+(t_{k+1}) \right\} + \frac{1}{2} \bar{a}^T(t_k) W \bar{a}(t_k) \quad (4-6)$$

where $\tilde{Y}(t_{k+1})$ is the observed signal and is defined in Chapter 2, $\hat{Y}^+(t_{k+1})$ is the calculated output vector, R^{-1} is a positive-definite covariance matrix, W is the weighting matrix and $\bar{a}(t_k)$ is the estimated model error vector (angular acceleration). To solve equation (4-6) $\hat{Y}^+(t_{k+1})$ is redefined in terms of angular rate and acceleration. Referring to Figure 4.1 $\hat{Y}^+(t_{k+1})$ is defined as the estimated output vector, with zero acceleration \hat{Y}_{k+1}^- , plus the product of the amount the output vector changes due to acceleration

$\frac{\partial \hat{Y}_{k+1}^+}{\partial \bar{a}_k} \bar{a}_k$. This is represented in mathematical form by

$$\hat{Y}^+(t_{k+1}) = \hat{Y}^-(t_{k+1}) + \frac{d\hat{Y}^-(t_{k+1})}{d\bar{a}(t_k)} \bar{a}(t_k). \quad (4-7)$$

Using the relationship for $\hat{Y}^+(t_{k+1})$ and minimizing equation (4-6) by determining the value of $\bar{a}(t_k)$ which gives stationary values of J leads to

$$\left\{ \tilde{Y}(t_{k+1}) - \hat{Y}^-(t_{k+1}) \right\}^T R^{-1} \frac{d\hat{Y}^-(t_{k+1})}{d\bar{a}(t_k)} + \bar{a}^T(t_k) \left(\left(\frac{d\hat{Y}^-(t_{k+1})}{d\bar{a}(t_k)} \right)^T R^{-1} \frac{d\hat{Y}^-(t_{k+1})}{d\bar{a}(t_k)} + W \right) = 0 \quad (4-8)$$

Solving equation (4-8) for acceleration, the deterministic model error vector is given by

$$\bar{a}(t_k) = \left(\left(\frac{d\hat{Y}^-(t_{k+1})}{d\bar{a}(t_k)} \right)^T R^{-1} \frac{d\hat{Y}^-(t_{k+1})}{d\bar{a}(t_k)} + W \right)^{-1} \left(\frac{d\hat{Y}^-(t_{k+1})}{d\bar{a}(t_k)} \right)^T R^{-1} \{ \tilde{Y}(t_{k+1}) - \hat{Y}^-(t_{k+1}) \} \quad (4-9)$$

For a deterministic attitude solution (i.e., a memoryless approach) the weighting matrix W is set to zero in equation (4-9).

4.3 Derivation and testing of the slope

In the model error vector equation (4-9), all terms are known except for the term, which

describes the amount $\hat{Y}^-(t_{k+1})$ changes with respect to acceleration, $\frac{d\hat{Y}^-(t_{k+1})}{d\bar{a}(t_k)}$. $\hat{Y}^-(t_{k+1})$

is explicitly dependent on the state vector $\hat{x}(\hat{q}, \bar{\omega})$, which in turn is explicitly dependent on $\hat{q}(\bar{\omega}, \bar{a}, t)$ and $\bar{\omega}(\bar{a}, t)$. With the knowledge of this dependency, the slope can be expanded using the chain rule to give

$$\frac{d\hat{Y}}{d\bar{a}} = \frac{\partial \hat{Y}}{\partial \hat{x}} \left\{ \frac{\partial \hat{x}}{\partial \hat{q}} \frac{\partial \hat{q}}{\partial \bar{a}} + \frac{\partial \hat{x}}{\partial \bar{\omega}} \frac{\partial \bar{\omega}}{\partial \bar{a}} \right\} \quad (4-10)$$

where

$$\frac{\partial \hat{x}}{\partial \hat{q}} = \begin{bmatrix} 1000 \\ 0100 \\ 0010 \\ 0001 \\ 0000 \\ 0000 \\ 0000 \end{bmatrix} \quad \text{and} \quad \frac{\partial \hat{x}}{\partial \bar{\omega}} = \begin{bmatrix} 000 \\ 000 \\ 000 \\ 000 \\ 100 \\ 010 \\ 001 \end{bmatrix}$$

To solve for $\frac{\partial \bar{\omega}}{\partial \bar{a}}$, take the partial derivative of the second term in equation (4-4), given

by

$$\frac{\partial \bar{\omega}_{k+1}}{\partial \bar{a}_k} = \frac{\partial (\bar{\omega}_k + \Delta t \bar{a}_k)}{\partial \bar{a}_k}$$

which results in

$$\frac{\partial \bar{\omega}}{\partial \bar{a}} = \begin{bmatrix} \Delta t & 0 & 0 \\ 0 & \Delta t & 0 \\ 0 & 0 & \Delta t \end{bmatrix}.$$

Since \hat{q}_{k+1} in equation (4-4) is an exponential matrix, the partial $\frac{\partial \hat{q}}{\partial \bar{a}}$ is more complicated.

In this problem, $\frac{\partial \hat{q}}{\partial \bar{a}}$ is solved two different ways. The first way that will be discussed is the method of expanding \hat{q}_{k+1} in a series before taking the partial derivative. The series expansion of \hat{q}_{k+1} is defined as

$$\hat{q}_{k+1} = \sum_{j=1}^{\infty} \frac{\left\{ \frac{\Delta t}{2} \Omega(\bar{\omega}_k) + \frac{\Delta t^2}{4} \Omega(\bar{a}_k) \right\}^j}{j!} \hat{q}_k.$$

The use of this method is important for possible future use on board a spacecraft. The number of floating point operations (FLOPS) required to compute a solution $\frac{\partial \hat{q}}{\partial \bar{a}}$ for a given accuracy is much less than the number of flops required using the functions in Matlab (ref. 8). Figure 4-2 below compares the exact solution of \hat{q}_{k+1} to a series expansion. Notice on the right-hand side of the plot, the text reads 1-Term, 2-Term, and 3-Term, this represents the number of terms retained in the series expansion. In Figure 4.2, there are two sets of lines for each term expansion.

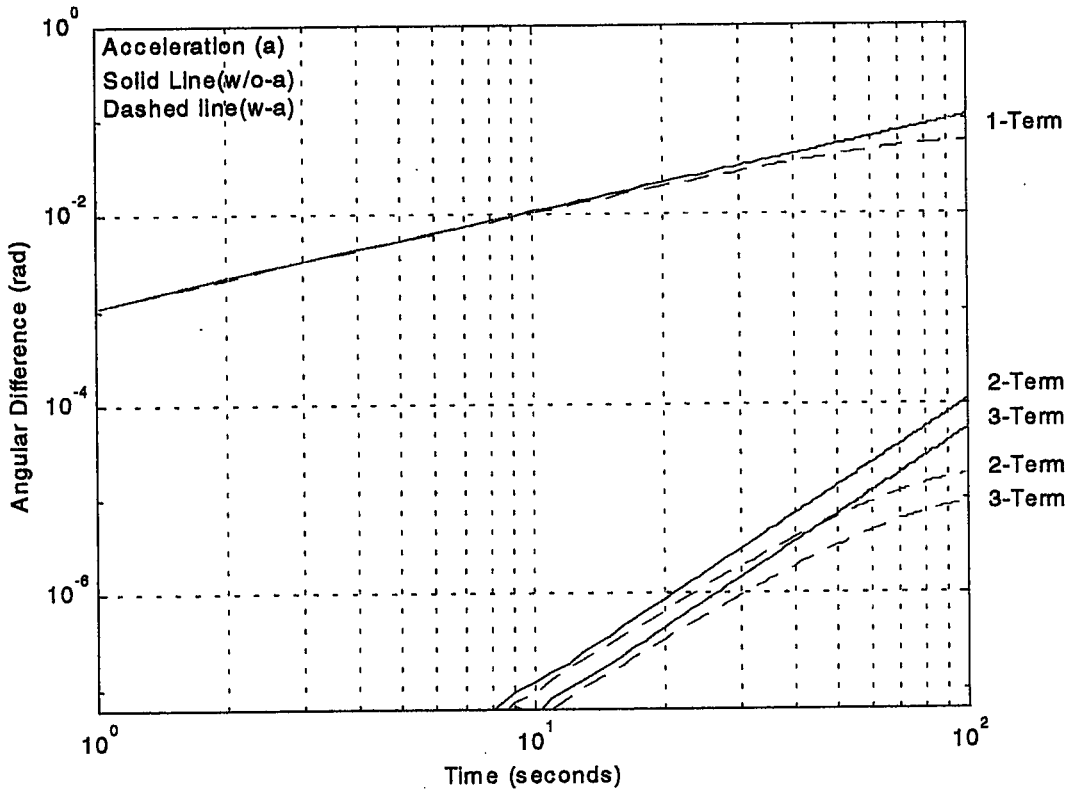


Figure 4.2 Comparison of accuracy of the series expansion

The solid line represents zero acceleration and the dashed line represents non-zero acceleration. Figure 4.2 shows the time interval between 1 and 100 seconds. The accuracy at which the quaternion is estimated improves with the addition of each term in the series expansion. Also notice that if a four term series expansion is used, the accuracy in estimating the state is less than $50\mu rad$ for both the solid and dashed line. This accuracy verses the number of FLOPs plotted in Figure 4.3. The number corresponding to each star represents the number of terms retained in the series expansion and the dashed line represent $50\mu rad$. The ODE45 and the Expm points at the bottom of the plot are the established functions used by Matlab (ref. 8). The accuracy with which these functions calculate the quaternions is considered exact at approximately 10^{-8} .

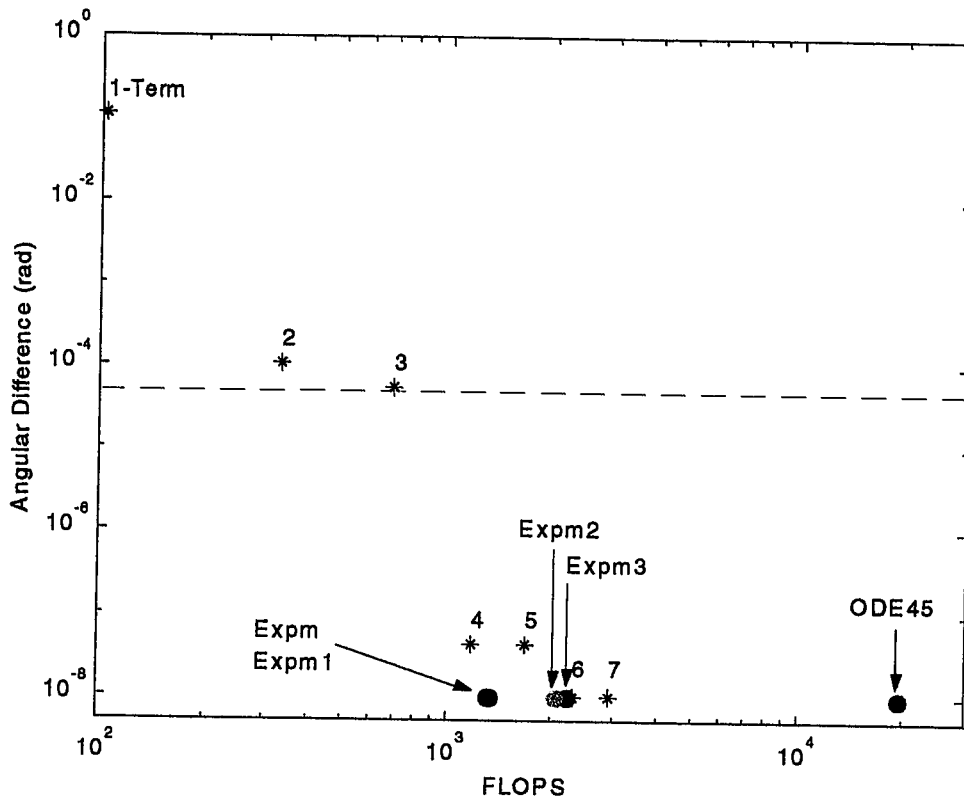


Figure 4.3 Effects of series truncation on accuracy

Notice that choosing a four term series expansion for the calculation of the quaternion gives a value within the required error range of $50\mu rad$ and the smallest number of FLOPS. The second method that will be discussed, is the direct calculation of $\frac{\partial \hat{q}}{\partial \bar{a}}$, given by

$$\frac{\partial \hat{q}_{k+1}}{\partial \bar{a}} = \frac{\partial \left(\frac{\Delta t}{2} \Omega(\bar{\omega}_k) + \frac{\Delta t^2}{4} \Omega(\bar{a}_k) \right)}{\partial \bar{a}} e^{\left(\frac{\Delta t}{2} \Omega(\bar{\omega}_k) + \frac{\Delta t^2}{4} \Omega(\bar{a}_k) \right)} \hat{q}_k$$

where \hat{q}_k , $\bar{\omega}_k$ and \bar{a}_k are all constant value, refer to Appendix A for an explanation on how to calculate these partial derivatives.

The accuracy of the finite difference solution is compared to the analytical solution. These solutions represent the slope or the change in the measurement ($d\hat{Y}$) with respect to the change in acceleration ($d\bar{a}$). Table 4.1 shows results of the two different methods for Δt of 100 seconds and 10 seconds. The constant values used to assemble Table 4.1 are

$$\bar{b}_3 = \begin{bmatrix} -3.93 \\ 3.93 \\ -1.23 \end{bmatrix}, \hat{s}_k = \begin{bmatrix} -0.6304 \\ -0.1491 \\ -0.7618 \end{bmatrix}, \dot{\hat{s}}_k = \begin{bmatrix} 0.7076 \\ 0.0109 \\ 0.0563 \end{bmatrix} \times 10^{-3}.$$

The above constant values are a set of values randomly chosen from the simulation data. As described, the angular rate is a linear function of acceleration and the quaternion is a non-linear function of acceleration. The initial values for the quaternion and angular rate are

$$\hat{q}_k = \begin{bmatrix} 0.8481 \\ 0.1380 \\ -0.4872 \\ 0.1557 \end{bmatrix}, [\bar{\omega}_k]_{ss} = \begin{bmatrix} 0 & 0 & -0.0011 \\ 0 & 0 & 0 \\ 0.0011 & 0 & 0 \end{bmatrix}.$$

The analytical solution is shown in equation (4-10) and is evaluated at zero acceleration. For the evaluation of the finite difference method, $d\hat{Y}$ was determined by evaluating equation (4-1) at zero acceleration and at a very small acceleration. The changes in acceleration, da , are listed in Table 4.1. The small change in acceleration is approximately 1% of the actual acceleration being seen by the spacecraft. In Table 4.1, each box is set up with a 2x3 matrix, the top row is change in phase and the bottom row is change in Doppler due to acceleration. As expected the phase difference is proportional to t^2 and Doppler difference is proportional to t . This would indicate that

the solution at 10 seconds would be exactly 1/100 of the phase and 1/10 of the Doppler at 100 seconds. These results are shown in Table 4.1.

Table 4.1 Comparison of the analytical solution verse finite difference solution

<i>Analytical solution</i>						
Delta-time:	100 Seconds			10 Seconds		
a = 0	16101	14446	-3744	166.84	157.63	-28.01
	308	279	-87	33.2	31.4	-5.7
<i>Finite difference solution</i>						
Delta-time	100 Seconds			10 Seconds		
da = 1.089e-7	16120	14449	-3745	166.84	157.63	-28.01
	304	260	-105	33.2	31.3	-5.9
da = 1.089e-8	16118	14446	-3748	166.84	157.63	-28.01
	304	260	-105	33.2	31.3	-5.9
da = 1.089e-9	16117	14445	-3748	166.84	157.63	-28.01
	304	260	-105	33.2	31.3	-5.9

The reason that the solutions are not exactly 1/100 or 1/10 is because the angular acceleration is not constant within the time step (refer to Figures 4.4 and 4.5). The actual acceleration is shown in the Figure 4.4.

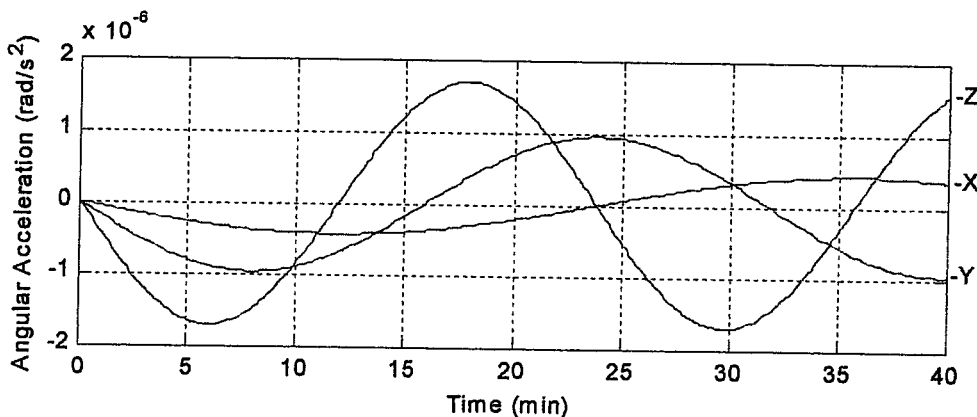


Figure 4.4 Simulated applied angular acceleration about all three axes

The angular acceleration, in Figure 4.4, is sinusoidal about all three axes and represents the angular acceleration applied to all the following case studies. Figure 4.5 represents the portion of Figure 4.4 between 0 and 100 seconds.

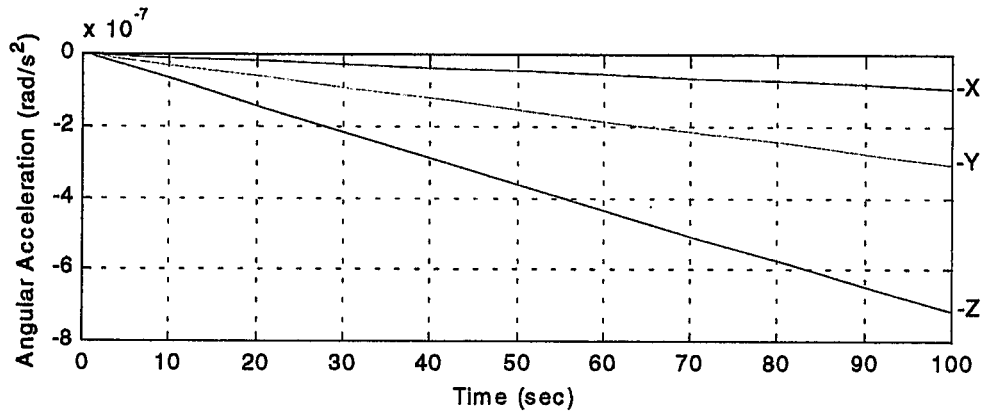


Figure 4.5 Simulated applied angular acceleration between 0 and 100 seconds

Figure 4.5 illustrates that the angular acceleration is not constant. Notice that the value, for all three components of angular acceleration, from 0 to 10 seconds is slightly different and from 0 to 100 seconds is dramatically different. This non-constant angular acceleration, within the time interval, represents the differences shown in Table 4.1. As stated early the values, shown in Table 4.1, at 10 seconds should be exactly 1/100 the phase and 1/10 the Doppler at 100 seconds. In future studies, the author recommends that the acceleration be assumed non-constant and the model error vector re-derived following the procedures outlined in this chapter.

Chapter 5 Nominal Case Study

In Chapter 5, a detailed description of the effectiveness of using the RARE algorithm to solve one of the most complicated cases will be discussed. This chapter should be referred to when reviewing the results of other case studies in Appendix B. Chapter 5 describes a low retrograde orbiting satellite, which is oscillating 5° about all three axes. The spacecraft is gravity gradient stabilized and has an orbital period of approximately 95 minutes.

5.1 Performance and accuracy

In section 5.1, the performance and accuracy of RARE, ALLEGRO, and the EKF are evaluated and compared. The standard deviation σ_p of the differential phase was chosen to be 0.026λ . This value of the standard deviation in phase is given by Crassidis as $\frac{RSS}{\lambda}$, where RSS is the total carrier phase error and λ is the wavelength of the carrier signal (ref. 1 and 9). The standard deviation σ_D , of the differential Doppler, was chosen to be $\sigma_D \approx \frac{2\sigma_p}{\Delta t}$. The standard deviation for Doppler is a crude estimation. As Δt increases, the differential Doppler decreases proportional to $\frac{1}{\Delta t}$ (ex. $\Delta t = 100$, $\sigma_D = 0.00052 \lambda/s$). The measured differential Doppler is between 10^{-4} to 10^{-3} . The standard deviation must be less than the measured values of differential Doppler for the STD to be used to calculate the angular rate of the spacecraft. If the standard deviation is greater than the measured differential Doppler, the measured differential phase will be the main contributor in the determination of the angular rate, which will be shown later

when ALLEGRO is discussed in section 5.1.3. The noise \bar{v} was selected from a uniform distribution with a variance $\sigma^2 = a^2/3$, where $\pm a$ is the range of the distribution about zero. The noise is created using a random number generator and a scaling factor of $2a_p$ (ex. $v_p = 2a_p(\text{rand} - 0.5)$, where $a_p = \sigma_p\sqrt{3}$). A similar equation for the noise in the differential Doppler can also be created using the a_D found from the standard deviation σ_D . The 10° error was determined by assuming that the initial guess of the quaternion is known to an accuracy of at least one wavelength. An average magnitude of one meter was chosen for the baseline vector and the wavelength of the GPS carrier signal is $\lambda = 0.19\text{m}$. The 10° error in the initial guess for the quaternion was chosen about the z-axis. The equation that relates the wavelength to the angular error is

$$\phi = \sin^{-1}\left(\frac{\lambda}{\|\bar{b}_1\|}\right).$$

The initial guess for the angular rate vector is chosen as the orbital frequency of the spacecraft.

5.1.1 RARE

Figure 5.1 illustrates how the algorithm RARE determines the quaternions (top plot), and angular rates (bottom plot) using the standard deviation $\sigma_D = 0.00052 \lambda/s$, zero data noise on the signal, and $\Delta t = 100$ seconds. This value of standard deviation in the differential Doppler corresponds to a standard deviation ratio of 1/50. The Standard Deviation (STD) ratio is defined as $\beta = \sigma_p / \sigma_D$. The actual accelerations are about all three axes, and are sinusoidal with different periods and amplitudes. For this case, the standard deviation of the angular position between the actual and calculated quaternions

is approximately $1.6\text{mrad}(0.0912^\circ)$. The standard deviation of the magnitude of the difference between the actual and calculated angular rates is $33\mu\text{rad}/\text{s}(0.0019^\circ/\text{s})$. The solution in RARE (solid line) does not follow the actual solution (dashed line) exactly because of the non-linearity in the acceleration. One of the main assumptions in deriving the predictive non-linear filter is the assumption that acceleration will be constant during the period between t_k and t_{k+1} .

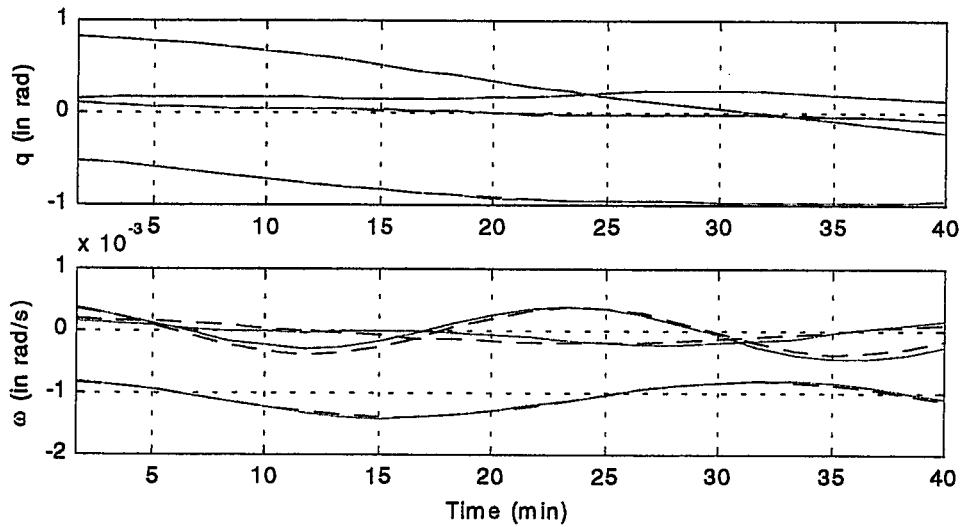


Figure 5.1 Evaluation of RARE without data noise and $\Delta t = 100$

Smaller time steps can be taken to more accurately track the non-linear behavior and align the RARE solutions with the actual results. The problem encountered with taking smaller time steps is that the standard deviation of differential Doppler increases. As mentioned early the method used to determine the standard deviation of differential Doppler is dependent on Δt . When $\Delta t = 10$, $\sigma_D = 0.0052$, 1/5 of the standard deviation in differential phase, and is on the same order as the measured differential Doppler. For this reason, the determination of angular rate will depend mainly on the differential phase

measurements rather than the differential Doppler measurements for short Δt 's. To illustrate how different STD ratios effect the estimation of both the quaternion and the angular rate, plots of angular position difference and magnitude of angular rate differences will be used. Angular position difference is determined by solving for the rotation that would be required to align the estimated quaternions to the actual. This is accomplished by first solving for the transformation matrix between the two states, given by

$$[\alpha_B] = [\alpha_C(\hat{q}_C)][\alpha_A(\hat{q}_A)]^T.$$

The subscript A represents the actual state, subscript C represents the calculated state, and the subscript B represents the transformation between A and C. The angular difference between the two states is then given by

$$\cos^{-1}\left(\frac{1}{2}(\text{trace}(\alpha_B)-1)\right).$$

The angular rate difference between the two states is given by

$$\|\bar{\omega}_C - \bar{\omega}_A\|.$$

All figures to follow will show the plots of the angular position and magnitude of angular rate differences using the previously explained criterion. The y-axis for the angular difference is in degrees, the y-axis for the magnitude of the angular rate difference is in degrees per second, and the x-axis is in minutes. All the studies will be based on $\Delta t = 100$ seconds. Results of parametric studies on the presence of noise on the differential phase and differential Doppler signal and on the error in the assumption of initial state, as described in section 5.1.1, will be presented.

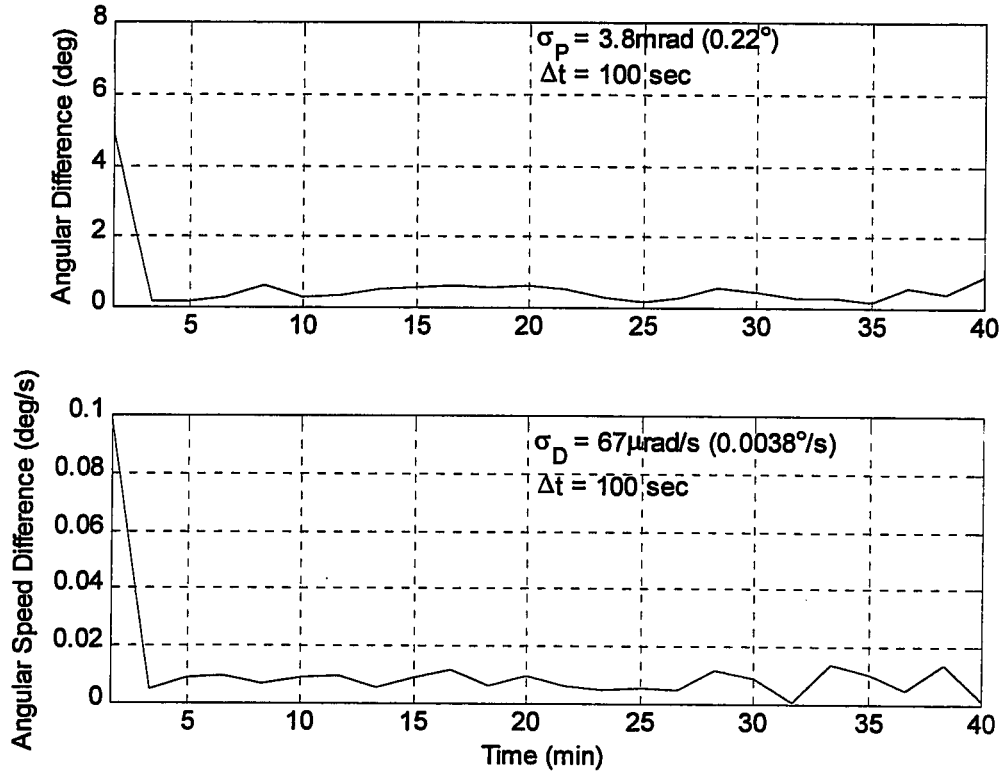


Figure 5.2 Performance of RARE with data noise and $\beta = 1/50$

In Figure 5.2 the standard deviation in the error for both the differences in angular position between the actual and calculated quaternions and the magnitude of the difference between the actual and calculated angular rate is shown.

In Figure 5.2, the standard deviation of differential Doppler is 1/50 the standard deviation of differential phase. Data noise on the same order is added to the system. Notice that the first calculated angular position difference is approximately 5° . Now recall that the initial quaternion guess had an error of approximately 10° . Figure 5.2 show that RARE estimates the first calculated quaternion within 5° of the actual. In Figure 5.1, where the state is being evaluated based on perfect inputs, the calculation of the state by the RARE algorithm is not perfect. For that case, the standard deviation of the angular position between the actual and calculated quaternions is approximately 1.6mrad (0.0912°). The

standard deviation of the magnitude of the difference between the actual and calculated angular rates is $33 \mu\text{rad}/s$ ($0.0019^\circ/s$). The results of a simulation with more emphasis placed on the calculation of the differential Doppler is shown in Figure 5.3. This increased emphasis was accomplished by decreasing the ratio between the standard deviation in differential phase and differential Doppler.

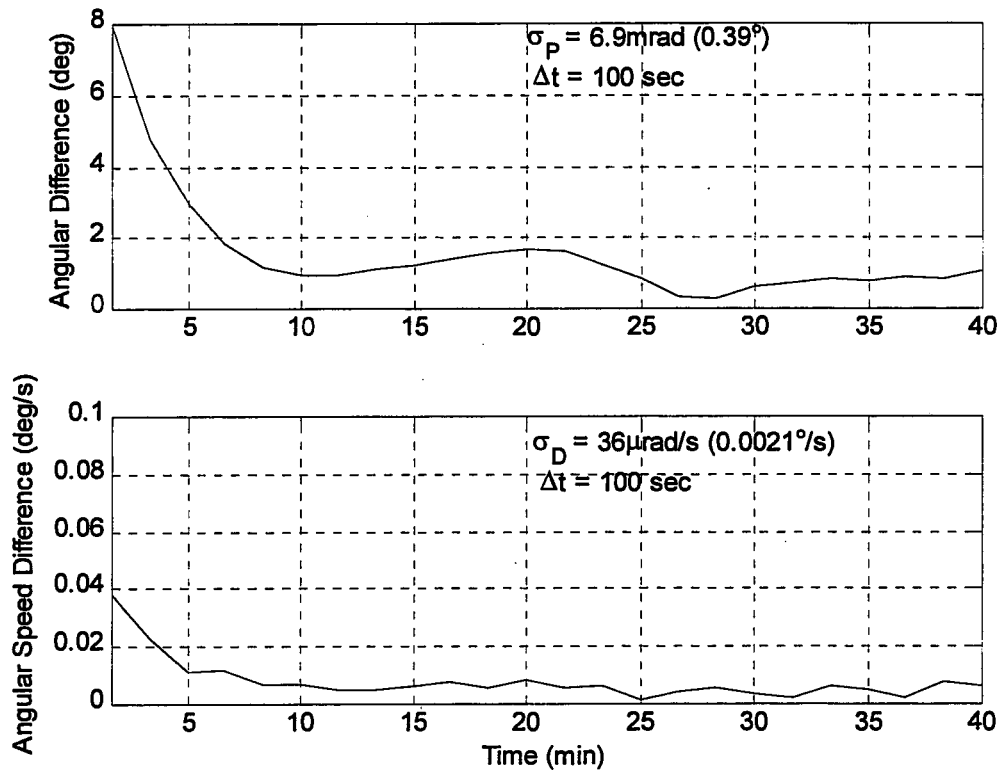


Figure 5.3 Performance of RARE with data noise and $\beta = 1/100$

The standard deviation of differential Doppler is assumed to be 1/100 the standard deviation of differential phase. The first calculated angular position difference is now approximately 8° . Notice by comparison of the results shown in Figure 5.2 and in Figure 5.3 that the calculation of angular rate has improved while the accuracy in determining the quaternion has decreased. In Figure 5.3, the value of the standard deviation for

determining \hat{q} has approximately doubled. This approximate factor of 2 can be accounted for from the ratios of the standard deviations. In Figure 5.2 the standard deviation in differential Doppler is 1/50 of the standard deviation of differential phase and in Figure 5.3 the ratio is half that value (1/100). The approximation in the factor of 2 is primarily due to the non-compliance of the assumption that acceleration is constant. The results shown in Figure 5.2 and 5.3 indicate that the calculation of attitude and angular rate is depended on the accuracy of the differential Doppler measurement. A future receiver must be capable of measuring differential Doppler to standard deviations approximately $\sigma_p / 100$. Data noise requirements to assure an angular rate recovery of 50 μ rad/s (approximately a 95% accuracy in the calculation) is shown in Figure 5.10.

5.1.2 ALLEGRO

In this section, results using ALLEGRO will be compared to the actual values of the quaternions and angular rates. ALLEGRO is only evaluated under two conditions. The first, in Figure 5.4, has no data noise and an exact initial state. The second is shown in Figure 5.5, with data noise and the initials values described in section 5.1.1. Since ALLEGRO does not utilize Doppler, the STD ratio will not be used. Also the standard deviation in phase is a scalar and has no effect on the covariance because in equation 2-10 the R matrix divides out to unity. The standard deviation in phase is only used for calculating the data noise on the phase measurements. In ALLEGRO the angular rate is the model error vector and is assumed constant over a computational sample time period. Figure 5.4 is shown to illustrate the similarities to Figure 5.1. ALLEGRO also shows an error in the determination of the angular rate vector under perfect conditions.

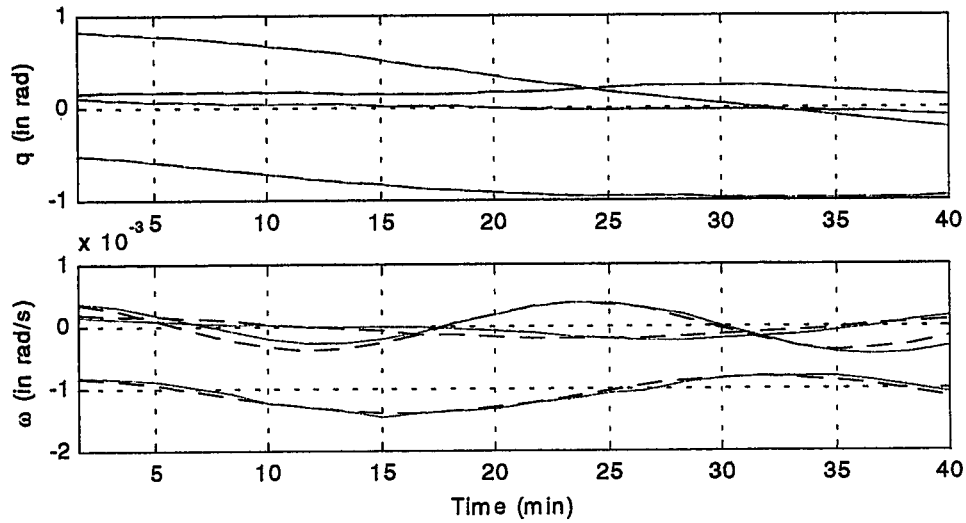


Figure 5.4 Performance of ALLEGRO with $\Delta t = 100$ and no data noise

The standard deviation of the magnitude of the difference between the actual and calculated angular rates is $39.6 \mu\text{rad}/s$ ($0.0023^\circ/s$). The performance when data noise is added to the differential phase measurement and an initial error is applied to the quaternion is shown in Figure 5.5. Notice that the first calculated angular position difference is approximately 0.3° and recall that the initial quaternion error was approximately 10° . The algorithm ALLEGRO converges quickly to almost within the standard deviation of the estimated values of the angular position differences.

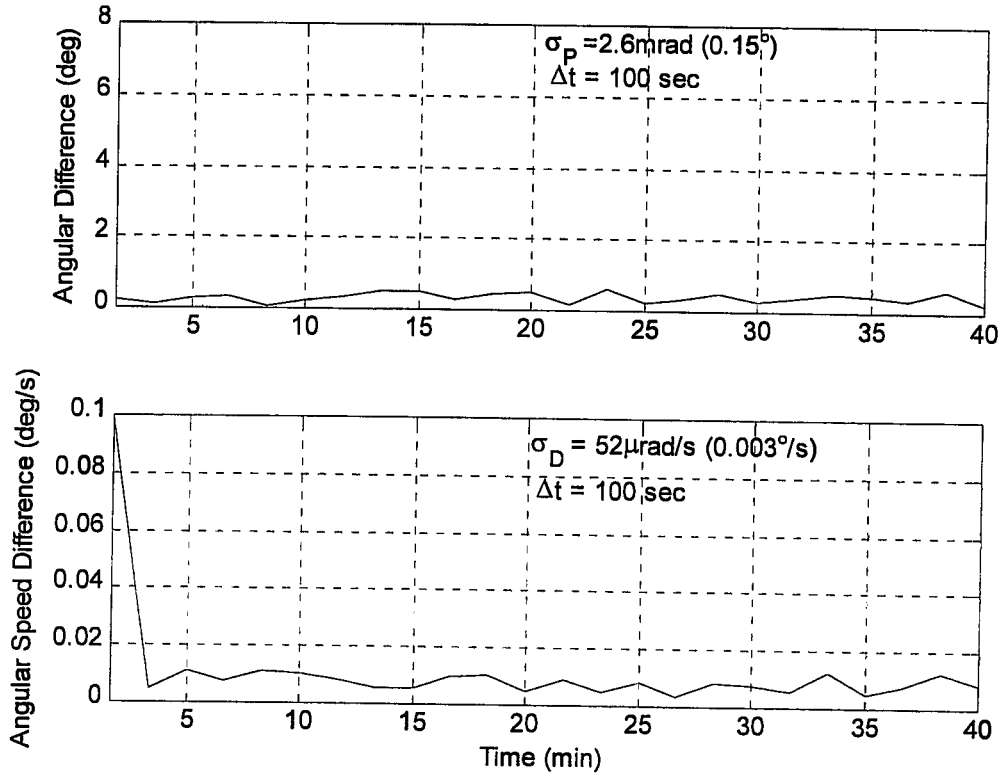


Figure 5.5 Performance of ALLEGRO with no data noise

The ALLEGRO algorithm is able to calculate the attitude and angular rate of the spacecraft even though one of the primary assumptions of constant angular rate is violated. The results shown in Figures 5.2, 5.3, and 5.5, indicate that the performance of RARE and ALLEGRO are very similar. These similarities are expected because both RARE and ALLEGRO assume a constant model error vector. As shown in section 4.3 the angular acceleration is not constant during the time interval Δt . Error is introduced into the determination of the model error vector for both RARE and ALLEGRO.

5.1.3 Extended Kalman filter

In this section, the extended Kalman filter will be discussed. The EKF requires a finely tuned Q_k matrix to optimize the results. The first case for the EKF is based on the perfect initial conditions and no noise on the data. For this case, the standard deviation of

the angular position between the actual and calculated quaternions is approximately $3\text{mrad}(0.17^\circ)$. The standard deviation of the magnitude of the difference between the actual and calculated angular rates is $9.1\text{rad}/s(0.00052^\circ/s)$. Notice that the results are not perfect. The results when data noise is added to the measured values, as described in section 5.1.2, is shown in Figure 5.6

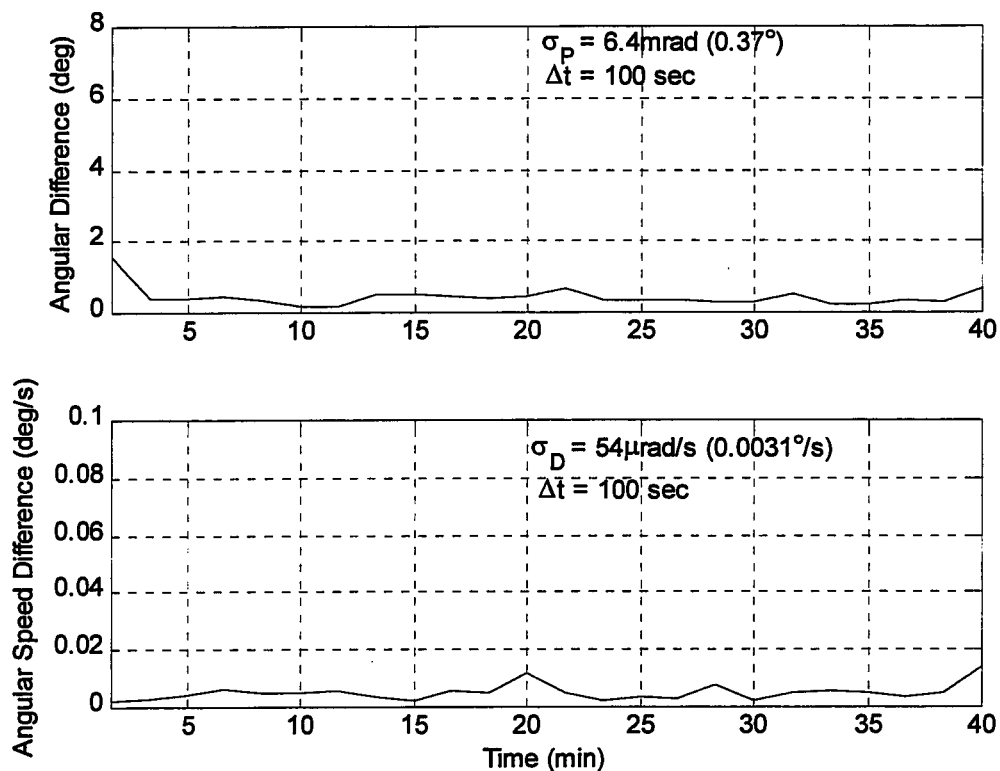


Figure 5.6 Performance of the EKF with data noise and $\beta = 1/50$

The standard deviation of differential Doppler for this calculation is $1/50$ the standard deviation of the differential phase. In Figure 5.6, notice that the first calculated angular position difference is approximately 1.5° and the first calculated magnitude of the angular rate difference is within the standard deviation. Figure 5.7 shows the

performance when the standard deviation of the differential Doppler is 1/100 the standard deviation of differential phase.

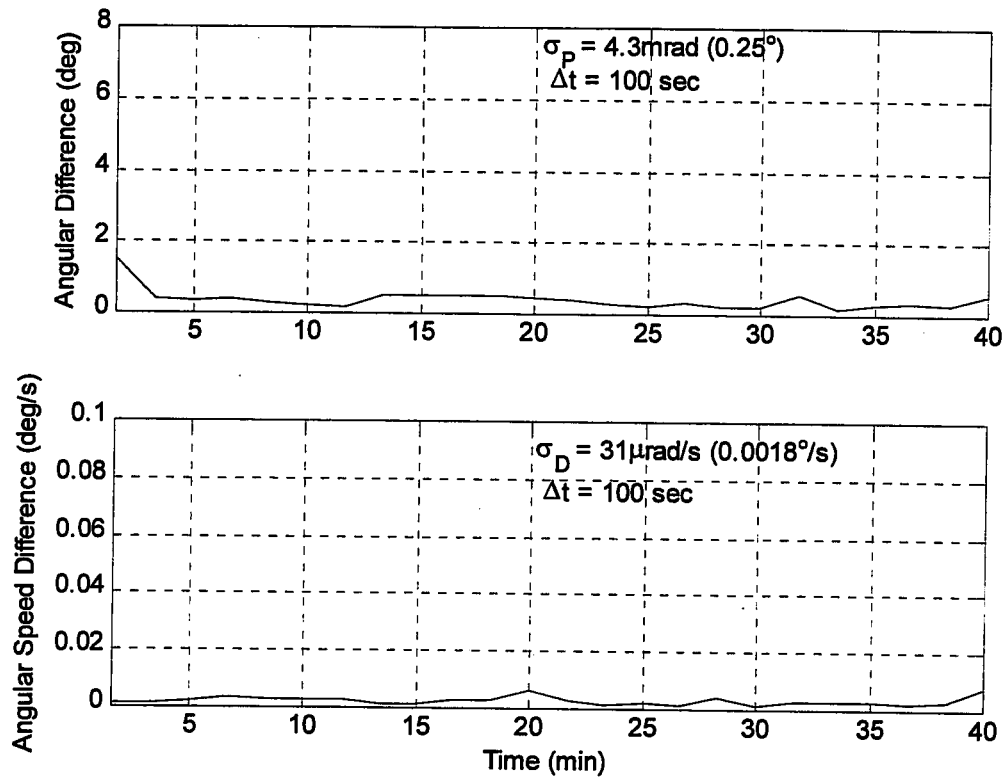


Figure 5.7 Performance of the EKF with data noise and $\beta = 1/100$

In Figure 5.7, the first calculated angular position difference is very similar to Figure 5.6. The first calculated magnitude of the angular rate difference is approximately the same as in Figure 5.6. The overall estimation of the angular rate shows improvement. It is recommended that the EKF be furthered studied and refined. With further studies and proper tuning of the Q_k matrix, the EKF should be able to return state estimations well within the desired parameters.

5.2 Convergence

In this section, a convergence study as a function of increased data noise will be discussed on all the algorithms. The discussion in section 5.2.1 will begin with the assumption that the data is measured exactly, i.e. the noise on the signal is zero. For the remaining sections, data noise will be added according to the standard deviation (STD) ratio ($\beta = \text{STD ratio}$). Figures with $\beta = 1/100$ are presented in earlier sections of Chapter 5. Figures with $\beta = 1/25$ are presented in this section. The setting of $\beta = 1/25$ corresponds to a large amount of data noise and $\beta = 1/100$ corresponds to a small amount of data noise. Results for all cases are computed over a time interval of 40 minutes.

5.2.1 RARE

Convergence is considered to have occurred when the calculated state is within the standard deviation, σ , initially assumed for differential phase and differential Doppler. Convergence for the angular difference plots is considered at approximately 1.5° . Convergence for the angular speed difference plots is considered at approximately 1.5β . In Figure 5.2, $\beta = 1/50$, there is data noise on the signal, and the initial state is given in section 5.1.1. The choice of the initial state will not change the calculation of standard deviation. The standard deviation is calculated after convergence has occurred. As shown in Figure 5.2, convergence occurs by the second time step ($2\Delta t$). In Figure 5.8, the standard deviation ratio is increased to $1/25$. The larger STD ratio places more weight on the differential phase measurement rather than differential Doppler. Notice in Figure 5.8 the time of convergence increases because of the addition of data noise. The convergence time is approximately 4 – 5 time steps. Also notice that the first calculated

angular position difference has improved over the previous cases shown in Figures 5.2 and 5.3 and the first and overall calculated angular speed differences have worsened.

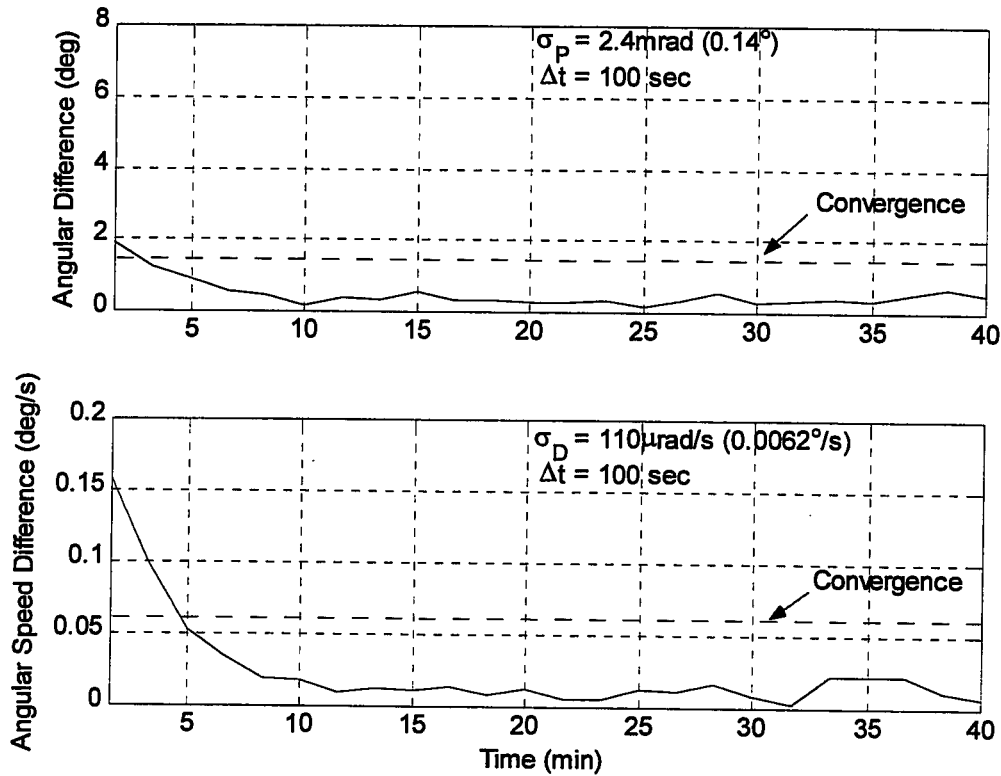


Figure 5.8 Convergence of RARE with data noise and $\beta = 1/25$

In Figure 5.3, both the angular difference and angular speed difference converge in about the same number of time steps as shown in Figure 5.8. The different STD ratio mainly affects the first calculated values and the STD's at convergence. In Figure 5.3 the first calculated value is approximately 8° for the angular difference and $0.04^\circ/\text{s}$ for the angular speed difference and the STD at convergence is 0.393° for the angular difference and $0.0021^\circ/\text{s}$ for the angular speed difference. Figure 5.8 shows that the first calculated value and the STD at convergence has improved for angular difference and has

worsened for angular speed difference. In general, the convergence is sensitive to the addition of data noise on the differential Doppler signal for the estimation of angular rate.

5.2.2 ALLEGRO

The convergence of ALLEGRO is indicated in Figure 5.5. Note that an initial guess for angular rate is not required for ALLEGRO. This algorithm estimates the angular rate and uses this estimation to calculate the attitude. In Figure 5.5 the first calculated value is approximately 0.3° for the angular difference and $0.1^\circ/s$ for the angular speed difference and the STD at convergence is 0.053° for the angular difference and $0.003^\circ/s$ for the angular speed difference. The model error vector effects the calculation of the quaternions through equation 4-4. The convergence of ALLEGRO is not affected by the STD ratio or the amount of noise on the differential Doppler measurement.

5.2.3 Extended Kalman filter

The convergence of the extended Kalman filter is evaluated using two different STD ratios. In Figure 5.7 the first calculated value is approximately 1.5° for the angular difference and $0.002^\circ/s$ for the angular speed difference and the STD at convergence is 0.249° for the angular difference and $0.0018^\circ/s$ for the angular speed difference. In Figure 5.9, the STD ratio is set to $1/25$. The EKF is also sensitive to the amount of data noise present on the differential Doppler signal as shown by comparison of Figure 5.7 and 5.9.

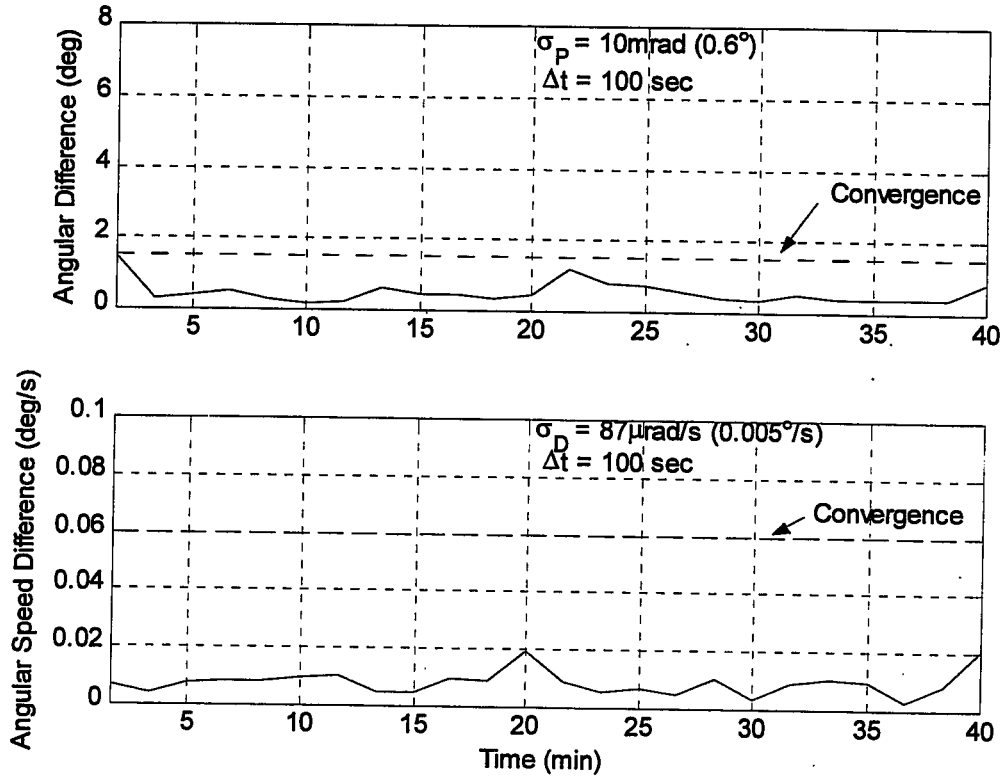


Figure 5.9 Convergence of the EKF with data noise and $\beta = 1/25$

5.3 Efficiency

In this section the efficiency of the algorithms will be evaluated. Efficiency is defined as a data noise region where the state is calculated with accuracies greater than $50 \mu\text{rad}/\text{s}$. To evaluate the efficiency, β is held constant and the data noise is varied for both the differential phase and differential Doppler signal. After each evaluation a standard deviation of the angular rate is calculated. If the resultant STD is less than or equal to $50 \mu\text{rad}/\text{s}$ the amount of data noise in each signal is stored in an array. This process was repeated for three different values of β . The arrays are then plotted for each set of covariance ratios (β). The data noise on the differential phase signal is evaluated between 0 and 0.1λ . The data noise on the differential Doppler signal is evaluated

between 0 and $5 \times 10^{-4} \lambda/s$. The three lines in Figure 5.10, representing the different covariance ratios, describe the data noise requirements to assure an angular rate recovery of $50 \mu rad/s$. The recovery requirements of $50 \mu rad/s$ correspond to about 95% accuracy in the calculation. Results of RARE are plotted with the results of ALLEGRO.

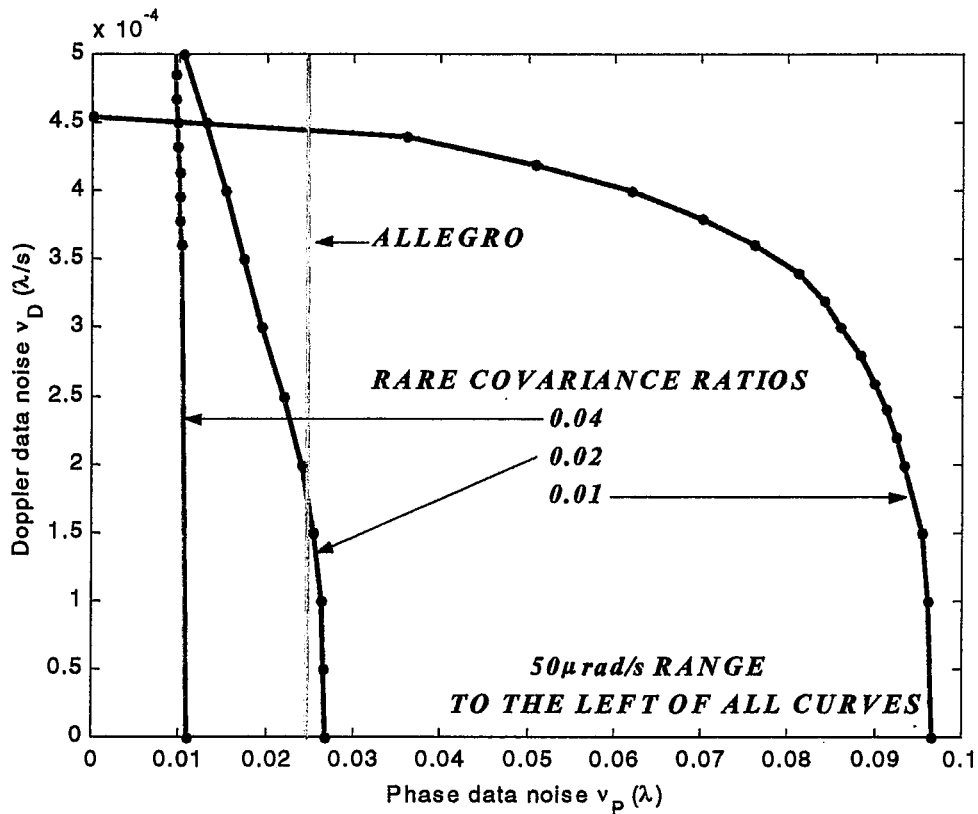


Figure 5.10 Data noise requirements in RARE to assure a $50 \mu rad/s$ rate recovery

Notice in Figure 5.10, that if the differential Doppler is measured with data noise approximately less than $4.5 \times 10^{-4} \lambda/s$, angular rate recovery is better than $50 \mu rad/s$.

In Figure 5.11, the extended Kalman filter is evaluated over the same ranges mentioned above and is also compared to ALLEGRO.

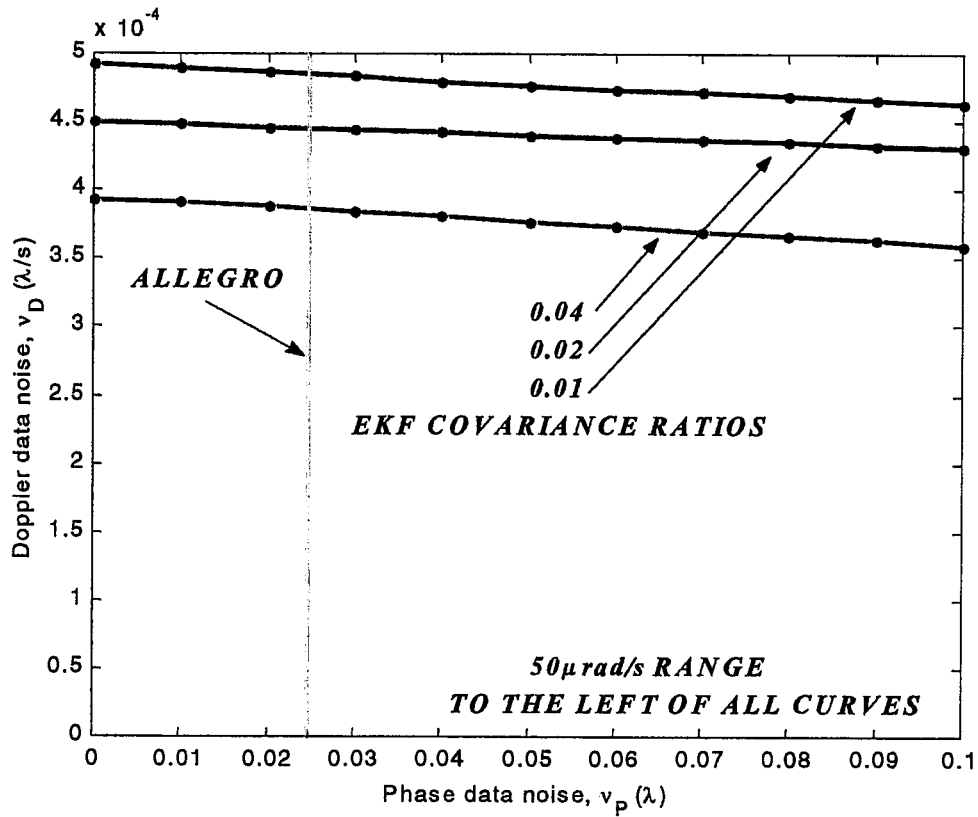


Figure 5.11 Data noise requirements in the EKF to assure a 50 μ rad / s rate recovery

The EKF allows a greater amount of error in differential Doppler and is not heavily influenced by the data noise in differential phase.

Chapter 6 Concluding Remarks

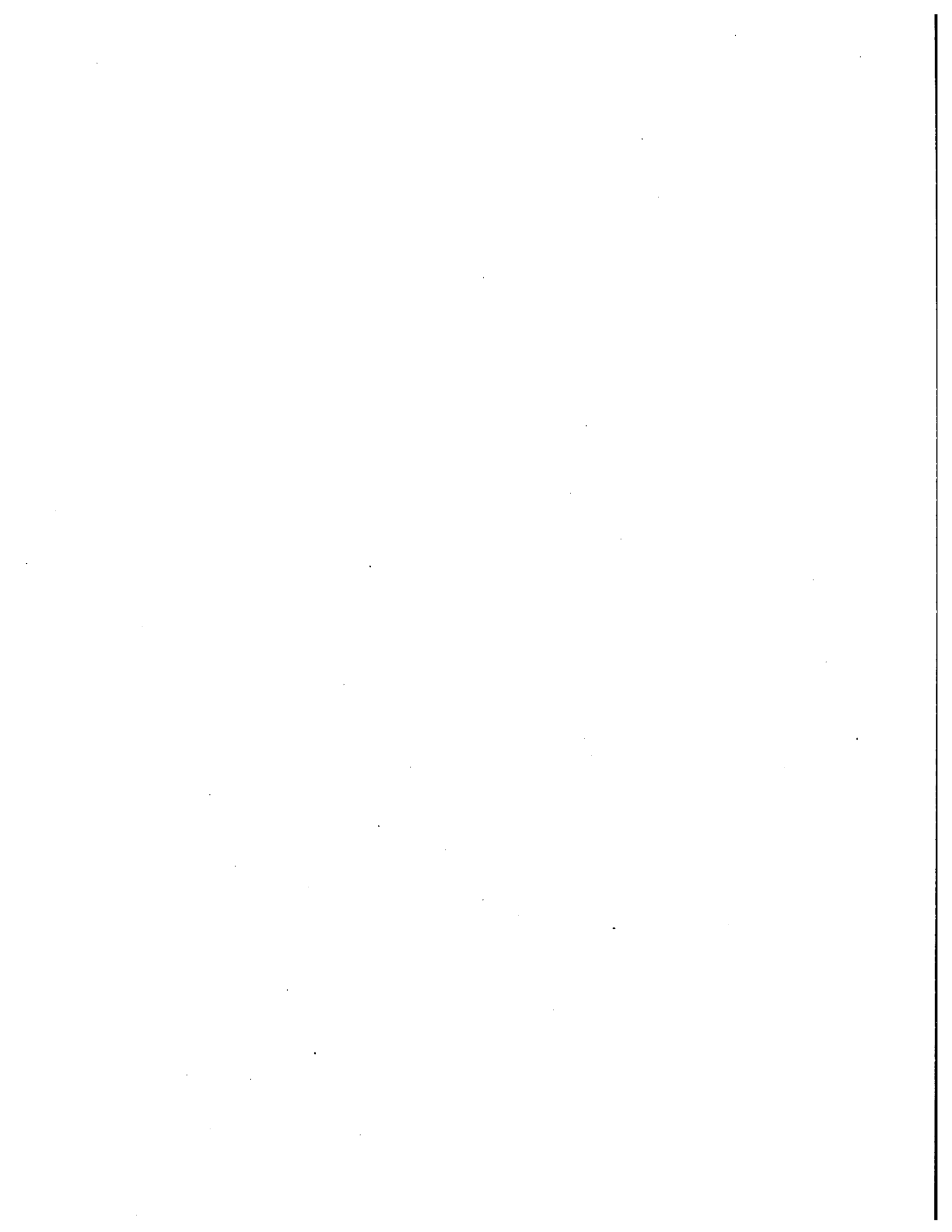
The ability to determine attitude and angular rate can be accomplished well with all the algorithms discussed in this paper. Each algorithm has advantages over the others for certain conditions. Though ALLEGRO is derived under the assumption that the angular rate is constant, it also performs well even when angular rate is no longer constant. While evaluating the efficiency of all the algorithms, it was shown that RARE is sensitive to the amount of data noise on the differential Doppler measurement. The calculation of attitude and angular rate is depended on the accuracy of the differential Doppler measurement. A future receiver must be capable of measuring differential Doppler to standard deviations approximately $\sigma_p/100$. With a differential Doppler standard deviation of $\sigma_p/100$, the state can be estimated, by the RARE algorithm, to a desired accuracy (greater than 95% as compared to actual state). The extended Kalman filter allowed for a greater error in the measured differential Doppler signal and little effect was contributed by the error in the measured differential phase signal. The results shown in this paper indicate that the algorithm RARE is depended on the accuracy in which the differential phase rate can be determined. The results also indicate that the extended Kalman filter returns the best estimates for attitude and angular rate.

In the derivation of the RARE algorithm, it was assumed that the acceleration was constant over each time step. For conditions where acceleration is not constant, non-linearity effects the estimation of the state. The algorithm includes the assumption that acceleration is constant over a specified interval. If acceleration cannot be assumed constant then the algorithm should be modified by retaining more terms in the series expansion of the solution. The addition of a weighting matrix in the RARE algorithm

would also be worthwhile. It is recommended that the EKF be furthered studied and refined. With further studies and proper tuning of the Q_k matrix, the EKF should be able to return state estimations well within the desired parameters.

References

1. Crassidis, J.L., Lightsey, E.G., and Markley, F.L., "Efficient and Optimal Attitude Determination Using Recursive Global Positioning System Signal Operations," *Journal of Guidance, Control, and Dynamics*, Goddard Space Flight Center, January 1, 1998
2. Crassidis, J.L., and Markley, F.L., "Predictive Filtering for Nonlinear Systems," *Journal of Guidance, Control, and Dynamics*, Vol. 20, No. 3, May-June 1997, pp. 566-572.
3. Brown, R.G., and Hwang, P.Y.C., "Introduction to Random Signals and Applied Kalman Filtering (2ed)," John Wiley and Sons, Inc., 1983, pp. 356-366.
4. Bar-Itzhack, I.Y., Deutschmann, J., and Markley, F.L., "Quaternion Normalization in Additive EKF for Spacecraft Attitude Determination," *Flight Mechanics/Estimation Theory Symposium*, National Aeronautics and Space Administration, Goddard Space Flight Center, May 1991.
5. Sheppard, S.N., "Quaternions from Rotational Matrix," *The Journal of Guidance and Controls*, Vol 1, No. 3, May – June 1973, pp. 223 –224.
6. Bates, R.R., Mueller, D.D., and White, J.E., "Fundamentals of Astrodynamics," Dover Publications, Inc., 1971 pp. 51-81.
7. Prussing, J.E., and Conway, B.A., "Orbital Mechanics," Oxford University Press, Inc., 1993, pp. 26-29 and pp.46-55.
8. Matlab, "The Language of Technique Computing," version 5.3.0.10183 (R11), Mathwork Inc.
9. Lightsey, E.G., Cohen, C.E., and Parkinson, B.W., "Application of GPS Attitude Determination to Gravity Gradient Stabilized Spacecraft," AIAA-93-3788-CP
10. Zwillinger, D., "Standard Mathematical Tables and Formulae 30th Edition," CRC Press, Inc., 1996, pp. 339-341.



Appendix A

Matrix and Vector Derivatives (ref. 10)

1. The derivative of the row vector \bar{y} with respect to the scalar x is

$$\frac{\partial \bar{y}}{\partial x} = \left[\frac{\partial y_1}{\partial x} \quad \frac{\partial y_2}{\partial x} \quad \dots \quad \frac{\partial y_m}{\partial x} \right].$$

2. The derivative of a scalar y with respect to the vector \bar{x} is

$$\frac{\partial y}{\partial \bar{x}} = \begin{bmatrix} \frac{\partial y}{\partial x_1} \\ \frac{\partial y}{\partial x_2} \\ \vdots \\ \frac{\partial y}{\partial x_n} \end{bmatrix}.$$

to \bar{x} is the Let \bar{x} be a $n \times 1$ vector and let \bar{y} be a $m \times 1$ vector. The derivative of \bar{y} with respect matrix

$$\frac{\partial \bar{y}}{\partial \bar{x}} = \begin{bmatrix} \frac{\partial y_1}{\partial x_1} & \frac{\partial y_1}{\partial x_2} & \dots & \frac{\partial y_1}{\partial x_n} \\ \frac{\partial y_2}{\partial x_1} & \frac{\partial y_2}{\partial x_2} & \dots & \frac{\partial y_2}{\partial x_n} \\ \vdots & \vdots & \ddots & \vdots \\ \frac{\partial y_m}{\partial x_1} & \frac{\partial y_m}{\partial x_2} & \dots & \frac{\partial y_m}{\partial x_n} \end{bmatrix}.$$

3. If \bar{x} and \bar{y} have the same length, then the absolute value of the determinant of $\frac{\partial \bar{y}}{\partial \bar{x}}$ is called the Jacobian of the transformation determined by $\bar{y} = \bar{y}(\bar{x})$.

4. The derivative of the matrix $A(t) = (a_{ij}(t))$, with respect to the scalar t , is the

$$\text{matrix } \frac{\partial A(t)}{\partial t} = \left(\frac{\partial a_{ij}(t)}{\partial t} \right).$$

Properties

y (scalar or a vector)	$\frac{\partial y}{\partial \bar{x}}$
$A\bar{x}$	A^T
$\bar{x}^T A$	A
$\bar{x}^T \bar{x}$	$2\bar{x}$
$\bar{x}^T A\bar{x}$	$A\bar{x} + A^T \bar{x}$

Quaternion Representation

In this paper the attitude matrix is assumed to be represented by the quaternion, defined as

$$\hat{q} = \begin{bmatrix} \hat{q}_{13} \\ q_4 \end{bmatrix}$$

with

$$\hat{q}_{13} = \begin{bmatrix} q_1 \\ q_2 \\ q_3 \end{bmatrix} = \begin{bmatrix} m_1 \\ m_2 \\ m_3 \end{bmatrix} \sin\left(\frac{\mathcal{G}}{2}\right)$$

$$q_4 = \cos\left(\frac{\mathcal{G}}{2}\right)$$

where m are the direction cosines of the Euler vector and \mathcal{G} is the angle of rotation.

The attitude matrix using the quaternion representation is given by

$$A(\hat{q}) = \Xi^T(\hat{q})\Psi(\hat{q})$$

with

$$\Xi(\hat{q}) = \begin{bmatrix} q_4 I_{3 \times 3} + [\hat{q}_{13} \times] \\ -\hat{q}_{13}^T \end{bmatrix}$$

$$\Psi(\hat{q}) = \left[\begin{array}{c} -q_4 I_{3 \times 3} + [\hat{q}_{13} \times] \\ \hline \hat{q}_{13}^T \end{array} \right]$$

where $I_{3 \times 3}$ is a 3x3 identity matrix, and $[\hat{q}_{13} \times]$ is a cross-product matrix because

$\hat{a} \times \hat{b} = [\hat{a} \times] \hat{b}$, with

$$[\hat{a} \times] = \begin{bmatrix} 0 & -a_3 & a_2 \\ a_3 & 0 & -a_1 \\ -a_2 & a_1 & 0 \end{bmatrix}.$$

Because a three-degree-of-freedom system is represented by a four-dimensional vector, the quaternion components cannot be independent of each other, which is shown by the following normality constraint

$$\hat{q}^T \hat{q} = \hat{q}_{13}^T \hat{q}_{13} + q_4^2 = 1$$

The matrix $\Xi(\hat{q})$ obeys the following helpful relationships

$$\begin{aligned} \Xi^T(\hat{q}) \Xi(\hat{q}) &= (\hat{q}^T \hat{q}) I_{3 \times 3} \\ \Xi(\hat{q}) \Xi^T(\hat{q}) &= (\hat{q}^T \hat{q}) I_{4 \times 4} - \hat{q} \hat{q}^T \\ \Xi^T(\hat{q}) \hat{q} &= \hat{0}_{3 \times 1} \\ \Xi^T(\hat{q}) \hat{\rho} &= -\Xi^T(\hat{q}) \hat{\rho} \text{ for any } \hat{\rho}_{4 \times 1} \end{aligned}$$

The matrix $\Psi(\hat{q})$ also obeys the equivalent relations in the above equations. Also,

other useful identities are given by

$$\begin{aligned} \Xi(\hat{q}) \hat{\omega}^V &= \Omega(\hat{\omega}^V) \hat{q} \text{ for any } \hat{\omega}_{3 \times 1}^V \\ \Psi(\hat{q}) \hat{\omega}^V &= \Gamma(\hat{\omega}^V) \hat{q} \text{ for any } \hat{\omega}_{3 \times 1}^V \end{aligned}$$

where

$$\Omega(\hat{\omega}^V) = \left[\begin{array}{c} -[\hat{\omega}^V \times] \\ \hline -\hat{\omega}^T \end{array} \middle| \begin{array}{c} \hat{\omega}^V \\ \hline 0 \end{array} \right]$$

$$\Gamma(\omega^{\mathbf{V}}) = \left[\begin{array}{c|c} -[\omega^{\mathbf{V}} \times] & -\omega^{\mathbf{V}} \\ \hline \omega^{\mathbf{T}} & 0 \end{array} \right]$$

Some useful relations for $\Omega(\omega^{\mathbf{V}})$ and $\Gamma(\omega^{\mathbf{V}})$ also include

$$\Omega(\omega^{\mathbf{V}})\Omega(\omega^{\mathbf{V}}) = -(\omega^{\mathbf{V}\mathbf{T}}\omega^{\mathbf{V}})I_{4 \times 4}$$

$$\Gamma(\omega^{\mathbf{V}})\Gamma(\omega^{\mathbf{V}}) = -(\omega^{\mathbf{V}\mathbf{T}}\omega^{\mathbf{V}})I_{4 \times 4}$$

Appendix B

Additional Case Studies

In Appendix B, three additional cases are introduced. The first case, similar to the case in Chapter 5, describes a low retrograde orbiting satellite, which is oscillating 1° about all three axes. The spacecraft is gravity gradient stabilized and has an orbital period of approximately 95 minutes. The second and third cases are also low retrograde orbiting satellites. These two cases describe a spacecraft that is normally inertially fixed and oscillating 1° about all three axes for the second case and 5° about all three axes for the third case. These cases are simulated over a 40 minute duration, $\Delta t = 100$ seconds, and with all the initial settings and guesses as presented in Appendix 5. This chapter will mainly present the resultant plots of each case study. All results are similar to those in Chapter 5. Additional important results not mentioned in the previous chapter will be stated.

B.1 Gravity gradient

As described above, all settings are the same as in Chapter 5. The standard deviation ratio will be evaluated at 1/50 and 1/100. Table B.1 will show the resultant standard deviations for a STD ratio of 1/50 and Figure B.1 will show the STD ratio of 1/100. The first case discussion is very similar to the case studied in Chapter 5. The case for a STD of 1/50 is shown in Table B.1. As seen in Figure 5.2, the results in Table B.1 have improved. The results for this case are expected because the algorithm RARE is estimating a smaller acceleration. The introduction of a smaller acceleration will lead to a greater accuracy in the results.

Table B.1 Performance of RARE with $\beta = 1/50$ and 1° oscillation

Standard Deviation \hat{q}	Standard Deviation $\bar{\omega}$
3.4mrad	57.1 μ rad/s
0.1949 $^\circ$	0.0033 $^\circ$ /s

In Figure B.1, the acceleration being applied is smaller and is as noticeable as in the acceleration being applied in Chapter 5. The estimation has improved as compared to Figure 5.3.

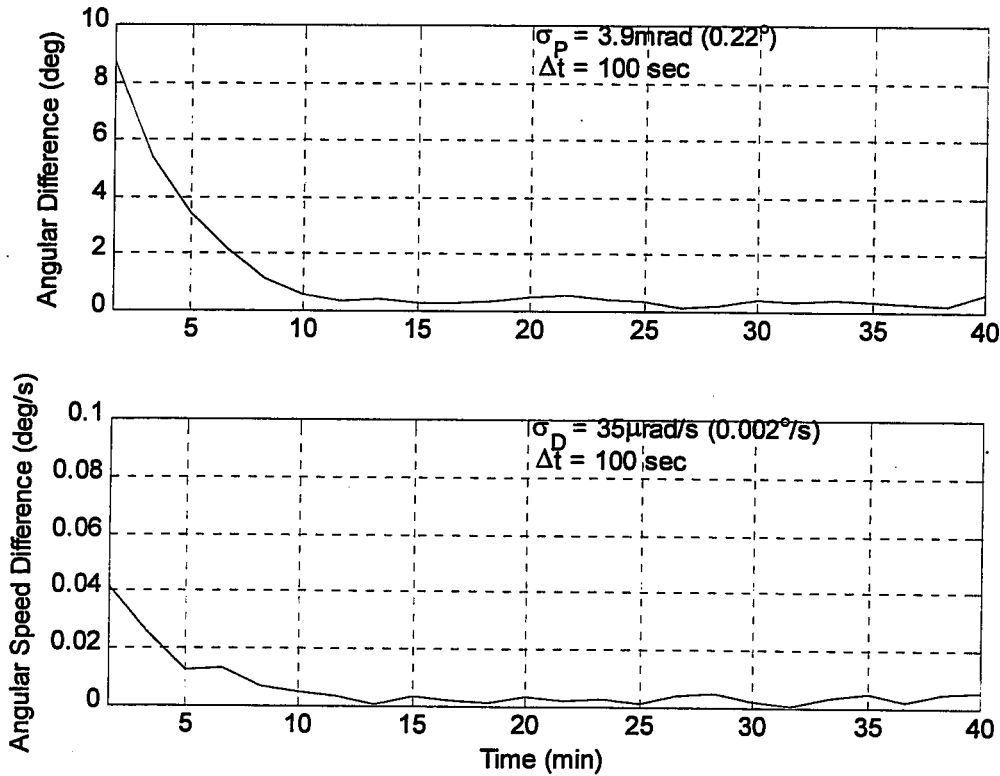


Figure B.1 Performance of RARE with $\beta = 1/100$ and 1° oscillation

The accuracy of the estimation of the algorithm RARE show an improvement in the determination of both the attitude and angular rate as expected. These results are consistent with an acceleration that is not constant (refer to the discussion in section 4.3.1

and 5.1.2). For both cases above, the algorithm RARE converges to the standard deviation recorded in Table B.1 and Figure B.2. In Figure B.2, the algorithm ALLEGRO shows an improved performance in the calculation of angular rate; refer to Figure 5.5. The improved performance is expected because the angular acceleration that is being applied to the angular rate is less.

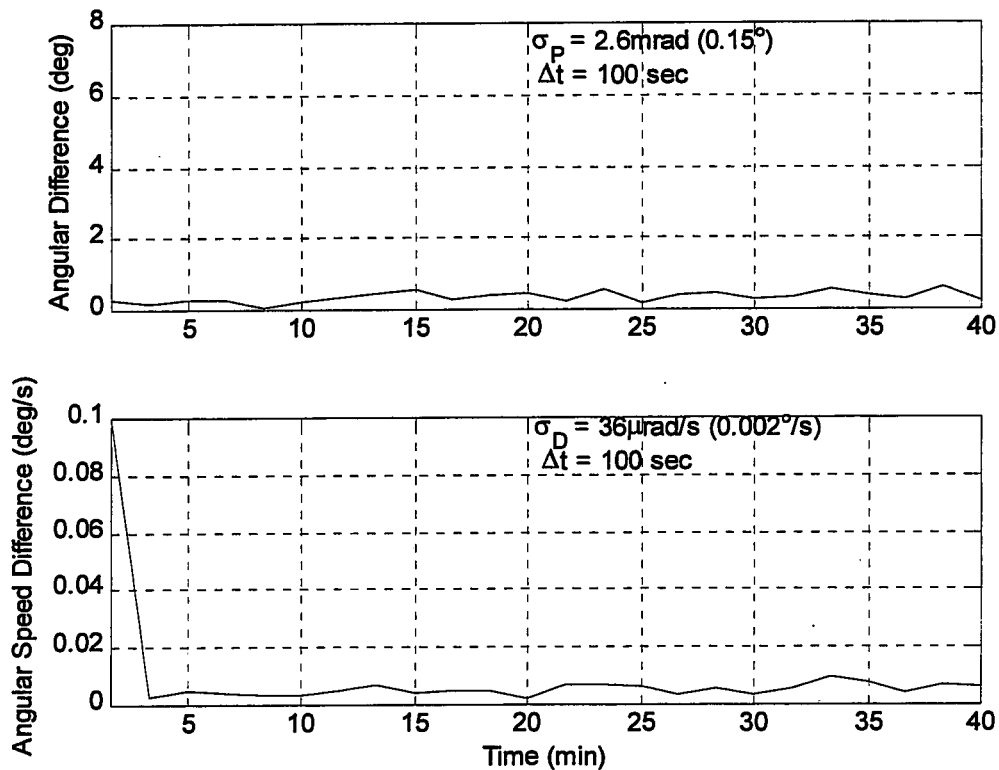


Figure B.2 Performance of ALLEGRO with 1° oscillation

The algorithm ALLEGRO is very efficient for estimating attitude with a constant angular rate (ref. 1). Table B.2 shows the performance of the EKF with a STD ratio of 1/50.

Table B.2 Performance of the EKF with $\beta = 1/50$ and 1° oscillation

Standard Deviation \hat{q}	Standard Deviation $\bar{\omega}$
4.72 mrad	53.5 μ rad / s
0.2706°	0.0031° / s

In Figure B.3, the STD ratio is decreased to 1/100. The overall results show that the extended Kalman filter is estimating the state with about the same accuracy. The improvement is mainly seen in the calculation of the attitude. A comparison should be made between the results shown in Figure B.3 and Tables B.2 and the results discussed in section 5.1.4.

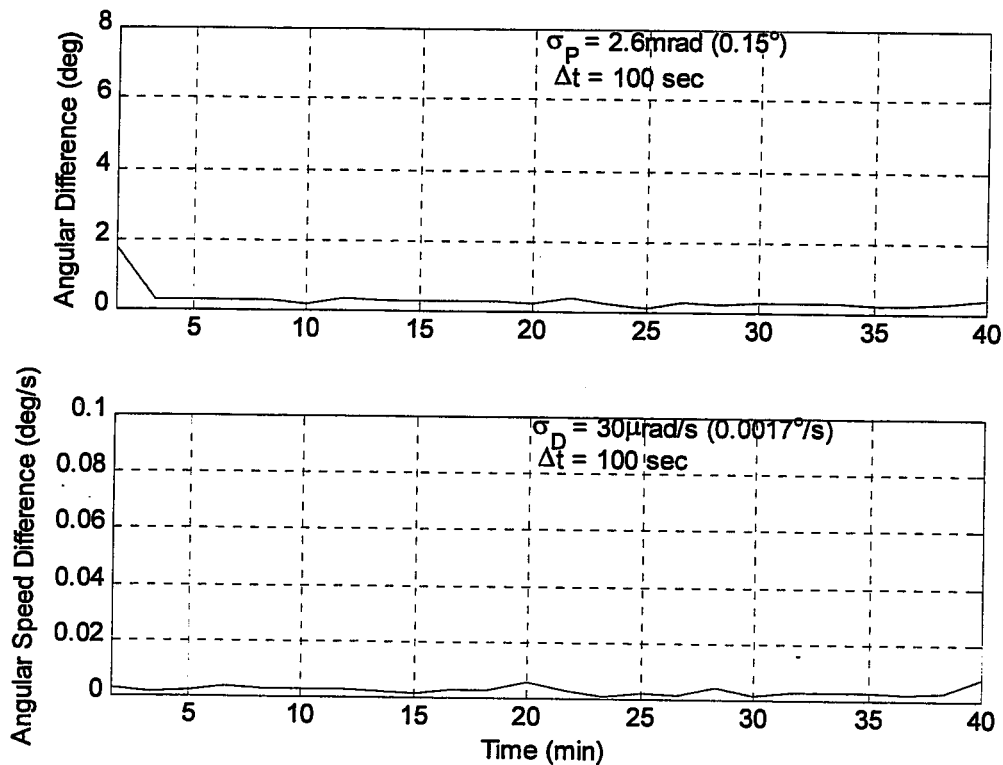


Figure B.3 Performance of the EKF with $\beta = 1/100$ and 1° oscillation

B.2 Inertially fixed

In this section, the case of an inertially fixed spacecraft will be presented. The first is a case similar to section B.1, 1° oscillation about all axes of the spacecraft. All results follow the same conditions presented in Chapter 5, but for a spacecraft that is inertially fixed.

B.2.1 Inertially fixed spacecraft oscillating 1° about all axes

Table B.3 represents the results using a STD ratio of 1/50. The overall results of this section show an additional improvement as compared to sections 5.1.2 and section B.1.1.

Table B.3 Performance of the RARE with $\beta = 1/50$ and 1° oscillation

Standard Deviation \hat{q}	Standard Deviation $\bar{\omega}$
2.11mrad	49.7 μ rad / s
0.1208°	0.0028° / s

In Figure B.4, the STD ratio is decreased to 1/100.

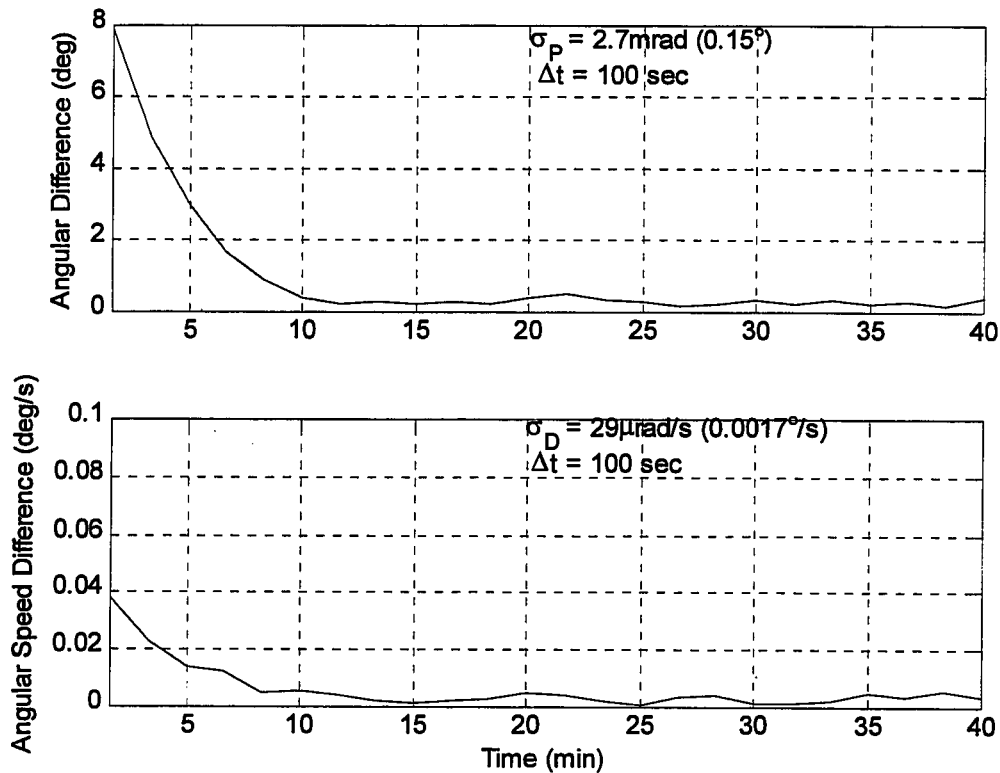


Figure B.4 Performance of RARE with $\beta = 1/100$ and 1° oscillation

Figure B.4 indicates a better estimation of the state as compared to Figure B.1. The inertially fixed case only requires the estimation of the acceleration and the effect it has on the state. The state vector for an inertially fixed spacecraft, under perfect conditions, has a zero angular rate and a constant attitude. Because of these previously mentioned conditions the estimation of the state for an inertially fixed spacecraft is expected to be better. In Figure B.5, ALLEGRO is evaluated for an inertially fixed spacecraft.

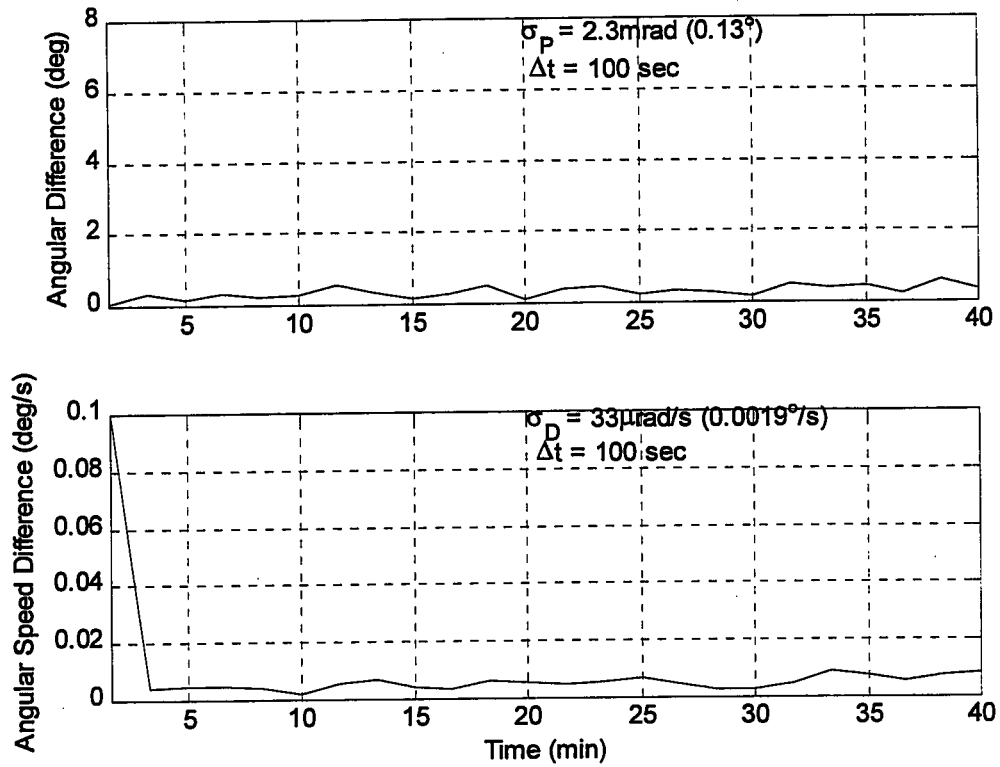


Figure B.5 Performance of ALLEGRO with 1° oscillation

ALLEGRO also show an improvement in the estimation of the state.

Table B.4 represents the results of the EKF using a STD ratio of 1/50.

Table B.4 Performance of the EKF with $\beta = 1/50$ and 1° oscillation

Standard Deviation \hat{q}	Standard Deviation $\bar{\omega}$
3.64 mrad	53.1 $\mu\text{rad} / \text{s}$
0.2086°	0.0030° / s

The STD ratio of 1/100 for the EKF is shown in Figure B.6.

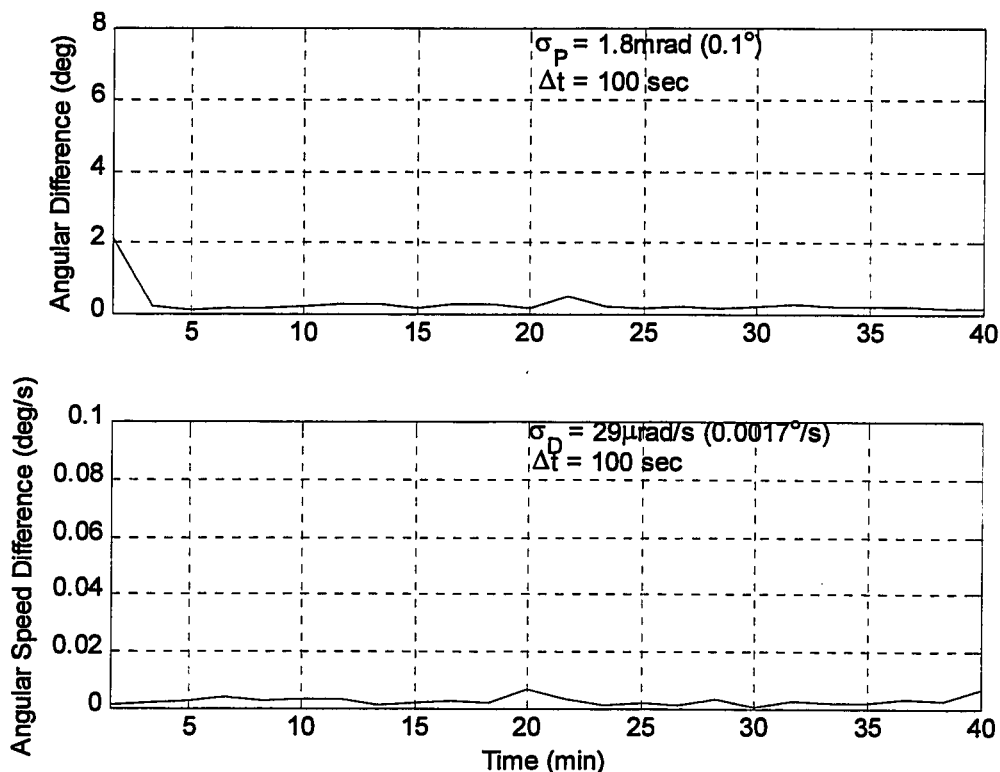


Figure B.6 Performance of RARE with $\beta = 1/100$ and 1° oscillation

The extended Kalman filter is also showing the same patterned discussed above.

B.2.2 Inertially fixed spacecraft oscillating 5° about all axes

In this section, the oscillation amplitude is increased to 5° about all axes for the inertially fixed case. The results seen in this section display the same patterns discussed throughout. The first case is shown in Table B.5 and represents the RARE algorithm with a STD ratio of 1/50.

Table B.5 Performance of RARE with $\beta = 1/50$ and 5° oscillation

Standard Deviation \hat{q}	Standard Deviation $\bar{\omega}$
2.27 mrad	51.8 μ rad / s
0.1298 $^\circ$	0.0030 $^\circ$ / s

In Figure B.7, the STD ratio is decreased to 1/100.

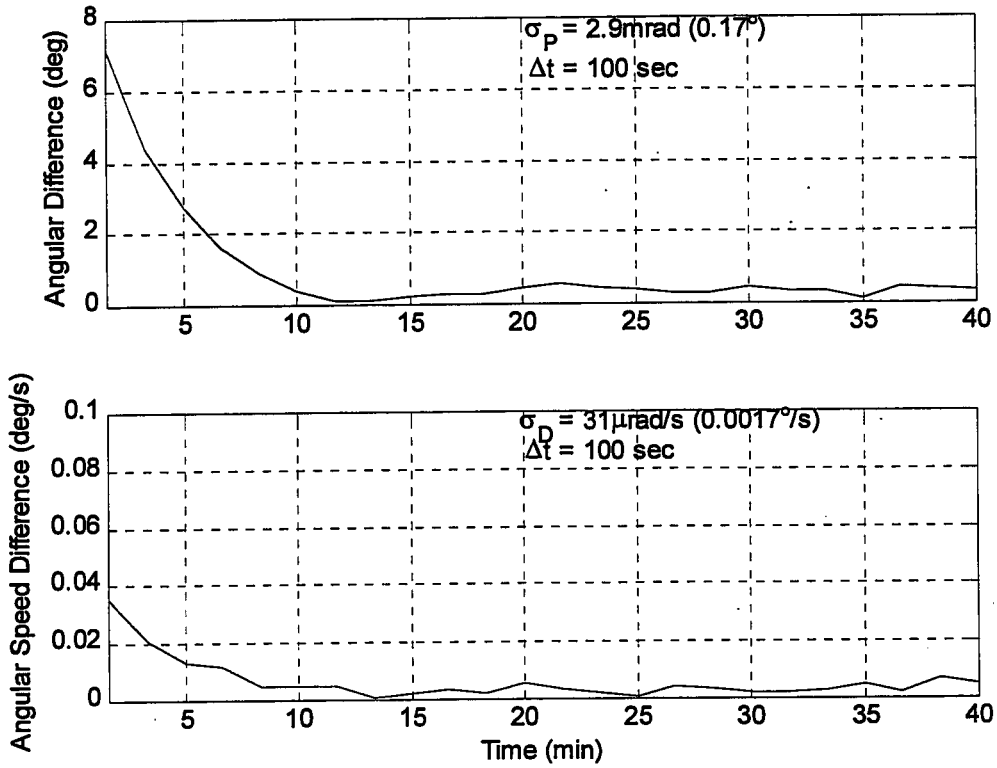


Figure B.7 Performance of RARE with $\beta = 1/100$ and 5° oscillation

In Figure B.8, ALLEGRO is evaluated for an inertially fixed spacecraft oscillating 5° about all three axes.

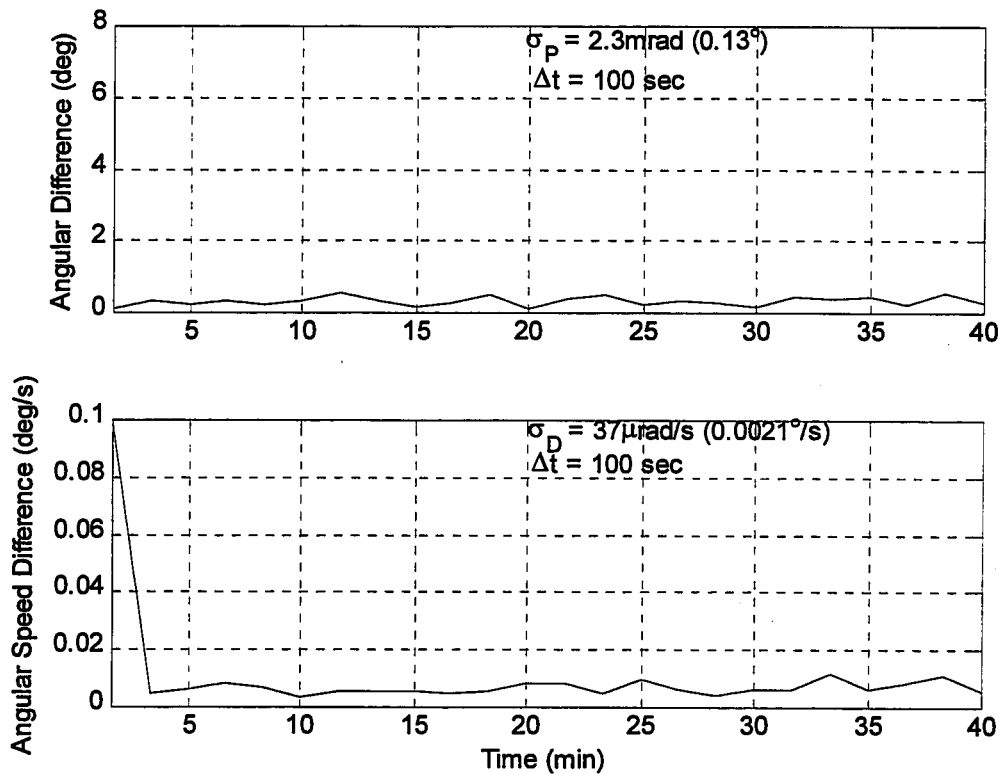


Figure B.8 Performance of ALLEGRO with 5° oscillation

The final case study is shown in Table B.5 and Figure B.9. Table B.5 describes an inertially fixed spacecraft oscillating 5° about all axes.

Table B.6 Performance of the EKF with $\beta = 1/50$ and 5° oscillation

Standard Deviation \hat{q}	Standard Deviation $\bar{\omega}$
5.53 mrad	56 $\mu\text{rad/s}$
0.3168°	0.0032°/s

In Figure B.9 the STD ratio is decreased to 1/100.

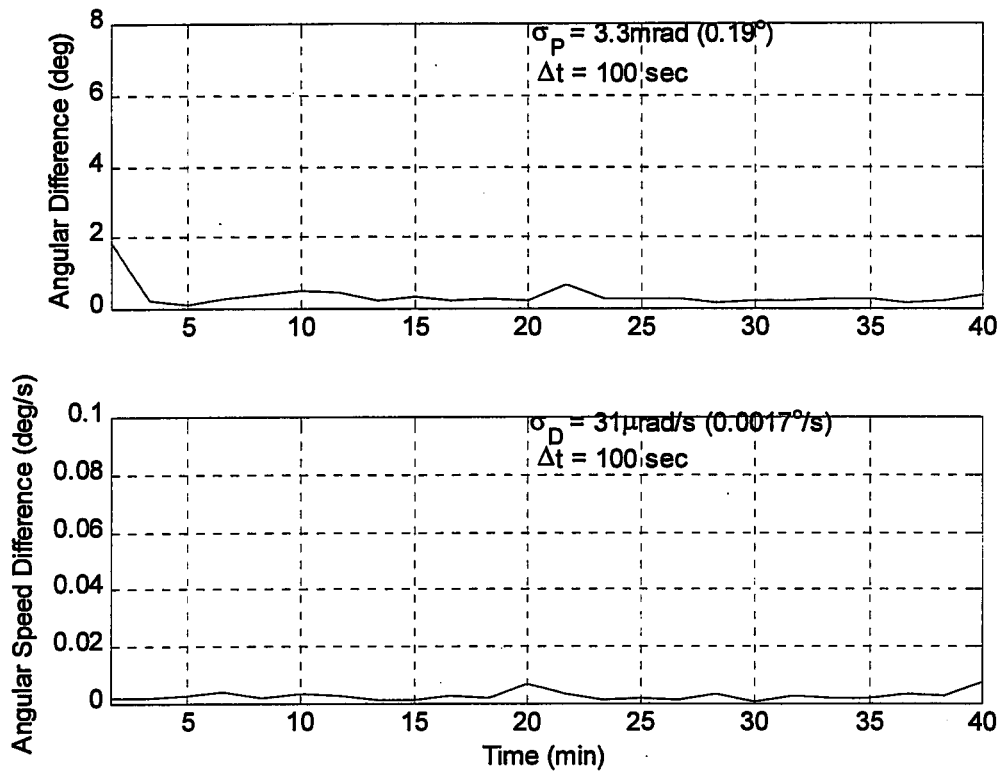


Figure B.9 Performance of the EKF with $\beta = 1/100$ and 5° oscillation